Review Vol. 13, No. 1 / January 2026 / Optica 143

OPTICA

Optical atomic clocks: defining the future of time and frequency metrology

Tara M. Fortier,[1,2,*] Andre N. Luiten,[3] and Helen S. Margolis[4]

[1]Time and Frequency Division, National Institute of Standards and Technology, Boulder, Colorado 80305, USA
[2]Time Department, Bureau International des Poids et Mesures, Sevres, France
[3]Institute for Photonics and Advanced Sensing and School of Physics, Chemistry and Earth Sciences, University of Adelaide, Adelaide, Australia
[4]National Physical Laboratory, Teddington, Middlesex TW11 0LW, UK
*tara.fortier@nist.gov

Received 11 August 2025; revised 5 December 2025; accepted 5 December 2025; published 16 January 2026

Optical atomic clocks based on laser-cooled trapped ions and atoms have advanced rapidly over the past decade. With fractional frequency uncertainties now surpassing 10^{-18}, they are some of the most precise measurement tools ever built. Yet researchers are still pursuing new avenues of research to explore the fundamental limits to their stability, accuracy, and reproducibility. In this mini-review, we provide a survey of the current state of the art by describing the fundamental principles and techniques that underpin this progress, the architectures used to realize optical clocks, and the supporting laser technologies that are essential to their operation. We also examine the progress that has been made toward a redefinition of the second in the International System of Units and the inclusion of optical clocks into the global time and frequency metrology infrastructure. Finally, we discuss emerging applications of optical clocks and look at the prospects for making their precision more readily accessible to end users.

https://doi.org/10.1364/OPTICA.575770

1. INTRODUCTION

While the philosophical nature of time remains elusive, the definition of a base unit of time has been pragmatically chosen to meet human needs. A universally agreed upon measure of time is essential for coordinating societal activities and enabling the seamless operation of communication, trade, and navigation systems, as well as for numerous scientific endeavors. This measure of time is set by the International System of Units (SI), in which the second is defined by fixing the unperturbed ground-state hyperfine frequency of the ^{133}Cs atom to be $\nu_{Cs} = 9,192,631,770$ Hz. This frequency can be regarded as a physical constant of nature, realized in practice with extraordinary accuracy through the construction and operation of an atomic clock.

This cesium atomic transition frequency has served as the basis for the internationally agreed definition since 1967, representing a conceptual advance on earlier astronomical definitions based on the periodicity of the Earth's rotation about its own axis or around the sun (ephemeris time) [1,2]. The period of the Earth's rotation around its axis is influenced by numerous processes including tidal forces, seismic activity, seasonal changes, and the melting of polar ice sheets [3], which result in short-term (one-year timescale) fluctuations at the millisecond level [4] making it inadequate as an accurate timekeeping standard.

The best microwave atomic clocks based on ^{133}Cs have reached an accuracy close to 1 part in 10^{16}, some six orders of magnitude better than the first practical cesium atomic clock developed in 1955 [5]. Today, there are around a dozen state-of-the-art cesium primary frequency standards around the world, being used in national UTC(k) time scales as well as to contribute data for computation of the globally agreed reference time scale Coordinated Universal Time (UTC) by the Bureau International des Poids et Mesures (BIPM) (Fig. 1).

While less precise than their optical counterparts, microwave atomic clocks remain compact, robust workhorses that support global positioning, telecommunications, and financial systems, and that continue to serve as time and frequency references in satellite navigation, space science, and timekeeping infrastructure. Atomic clocks lie at the heart of global navigation satellite systems (GNSS), enabling users to determine location through time-of-flight measurements between satellites and receivers. Today, GNSS supports a huge range of industries from logistics and agriculture to autonomous systems and precision surveying.

The focus of this review, however, is on next-generation optical atomic clocks. These offer a natural path to better fractional frequency stability thanks to their much higher operating frequencies. Since the 1990s, optical clock accuracy has seen greater than a factor of a 100 times improvement per decade (Fig. 2) enabled by breakthroughs in laser science, nonlinear optics, quantum control, and frequency metrology, many of which are recognized in the timeline of Nobel Prizes that trace the field's evolution [6–21]. The most advanced optical atomic clocks now achieve a measurement uncertainty below 1 part in 10^{18} [22,23], making them some of the most precise measurement tools ever built. With performance now surpassing Cs primary standards by two orders of magnitude, these

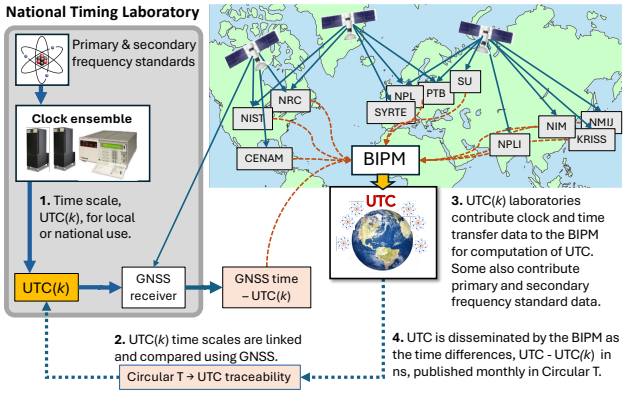

Fig. 1. Coordinated Universal Time (UTC) is computed from about 450 atomic clocks in nearly 85 laboratories worldwide. Most are commercial cesium clocks or hydrogen masers that operate continuously to generate local time scales, UTC(k), which are disseminated via internet servers, radio, cell towers, or fiber networks. Some labs use primary or secondary standards to calibrate these clocks against the SI second. UTC is determined from comparisons between UTC(k) time scales using various time transfer methods—most commonly GNSS, due to its accessibility, global reach, and low cost. The BIPM processes clock and time transfer data to produce a stable UTC time scale, whose rate is aligned with the SI second. Monthly, it publishes Circular T, listing the time differences between each UTC(k) and UTC, providing traceability and a slow correction signal for local scales.

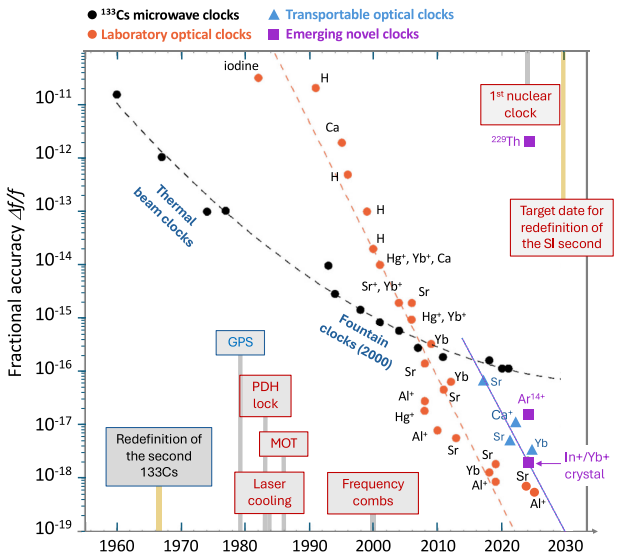

Fig. 2. Advances in microwave (^{133}Cs) and optical atomic clock accuracy over time. The figure also highlights key technological milestones that have enabled improvements in clock performance, including: laser cooling (Section 3.A); the development of the magneto-optical trap (MOT) for cooling and trapping neutral atoms (Section 4.B); the Pound–Drever–Hall (PDH) locking technique for stabilizing lasers to sub-Hz linewidths (Section 5.A); and optical frequency combs (Section 5.B), which provide traceability to the SI second and enable direct frequency comparisons across the optical spectrum.

capabilities are expected to drive a redefinition of the second in the coming decade [24], this time in terms of an optical transition or transitions.

Detailed reviews of optical clocks have been published previously, for example [25,26]. In this mini-review, we focus on their key features, progress over the last decade and other recent developments, which we consider particularly promising for the future. We begin with a tutorial-style introduction describing the operation of a simple optical atomic clock along with the supporting optical systems that make optical clocks possible. The accompanying discussion is centered around three related avenues of research with distinct but related objectives:

1. Advancing optical clock performance to explore the fundamental limits to their stability, accuracy, and reproducibility.
2. Incorporating optical clocks into the global time and frequency metrology infrastructure, to improve the stability and accuracy of the global reference time scale UTC and drive progress toward a redefinition of the second.
3. Making optical atomic clocks more accessible to end users, enabling their widespread use, and stimulating new applications.

2. OPTICAL ATOMIC CLOCK BASICS

A key to the success of atomic clocks and atomic sensors lies in the extraordinary properties of atoms as references: (1) **reproducibility**: all atoms of a given isotope have an identical energy level structure, and this structure is believed to be invariant in time and space, being governed by unchanging physical laws, (2) atoms are also **abundant and universally available**, and (3) **control:** atoms can be well isolated from their environment, with the internal interactions between the electrons and the nucleus strongly dominating over external perturbations.

While microwave clocks and optical clocks are operationally similar, the main difference lies in their transition frequency. Microwave clocks operate at gigahertz frequencies, and optical clocks operate closer to the petahertz regime.

A simplified view of how an optical atomic clock works is shown in Fig. 3. Just as in a microwave atomic clock, the frequency of an oscillator is stabilized to an atomic reference transition, but in this case the oscillator is a laser, and the reference is a narrow optical transition. Although not usual in practice, absorption spectroscopy offers a conceptually simple way to understand how one could lock the frequency of a laser onto that of an atomic transition. One can shine the laser at a cloud of atoms, and only when it is resonant with the atomic transition will it be absorbed. A photodetector monitoring the laser transmission through the sample will record a varying voltage as the frequency of the laser is tuned through resonance. The signal can be processed to produce an error signal that shows whether the laser frequency is too high or too low. This error signal is then used in a feedback loop to keep the laser locked to the atomic transition.

This frequency-stabilized oscillator provides the optical output of the atomic clock, carrying the stability and accuracy of the atomic resonance within the timing of its electromagnetic cycles. Because optical signals cycle too fast to be counted directly, a frequency comb (Section 5.B) can be used to divide the optical signal to the radio frequency (RF) domain, enabling its frequency to be determined relative to a cesium primary frequency standard (i.e., measured in hertz using a commercial frequency counter). The optical clock thus produces two phase-coherent outputs, one optical and one radio frequency, either of which can serve as a frequency reference for measuring and characterizing other signals, or for other applications.

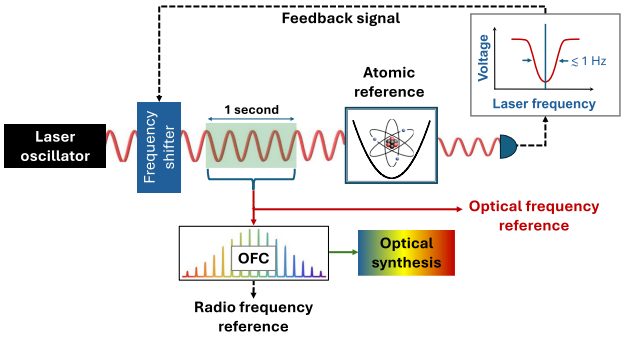

Fig. 3. Simplified schematic of an optical atomic clock. A laser is locked to a narrow atomic transition using absorption spectroscopy, which produces a frequency-dependent error signal. The stabilized laser output serves as an optical frequency reference that is sent to an optical frequency comb (OFC). The OFC coherently synthesizes a broadband optical spectrum from the atomic reference and downconverts the stabilized optical signal, producing a radio frequency domain output whose frequency can be precisely evaluated using commercial frequency counters. In state-of-the-art systems, atoms are laser-cooled and trapped to suppress motion-induced shifts, while less precise clocks may use thermal atoms or atomic beams.

A. Clock Performance: Accuracy, Precision, and Stability

The performance of an optical atomic clock depends on several factors: (1) the atomic transition used as the frequency reference, (2) the quality of the oscillator used to probe this transition, and (3) the isolation of the atomic sample from its environment.

In time and frequency metrology, performance is commonly quantified using the Allan deviation (ADEV) [27,28]. It is the standard tool for analyzing noise processes that vary across timescales and complements accuracy metrics that describe systematic offsets from the unperturbed transition frequency.

As illustrated in Fig. 4, clock performance encompasses several distinct measures. Let us define the fractional-frequency deviation $y(t) = \frac{f(t)-f_0}{f_0} = \varepsilon + \delta(t)$, where ε is the long-term average of $y(t)$ (the fractional inaccuracy of the clock) and $\delta(t)$ represents the zero-mean, time-varying fluctuations. A simple standard deviation assumes stationary noise and a well-defined mean, whereas the Allan deviation instead computes differences between successive averages of $y(t)$ taken over intervals of duration τ. Evaluating $\sigma_y(\tau)$ over a range of τ reveals how a clock's frequency stability evolves with averaging time. Because ADEV remains meaningful even in the presence of long-term noise processes such as flicker or random-walk behavior, it is widely used as a robust measure of clock instability.

B. Advantage of Optical Clocks

A major advantage of optical clocks is their much higher transition frequencies, which translate into higher quality factors, $Q = f_0/\Delta f$, where Δf is the width in which the response drops by 3 dB from its peak value. The quality factor characterizes the sharpness of the atomic transition, which fundamentally limits the frequency resolution achievable in a clock. Since clock instability scales inversely with the quality factor of the reference transition, this suggests a potential improvement in stability of up to $\sim 10^5$ compared to cesium primary standards operating at 9.2 GHz. In practice, however, the realized improvement is more modest due to technical and quantum-limited noise sources, as discussed in Section 3.C.

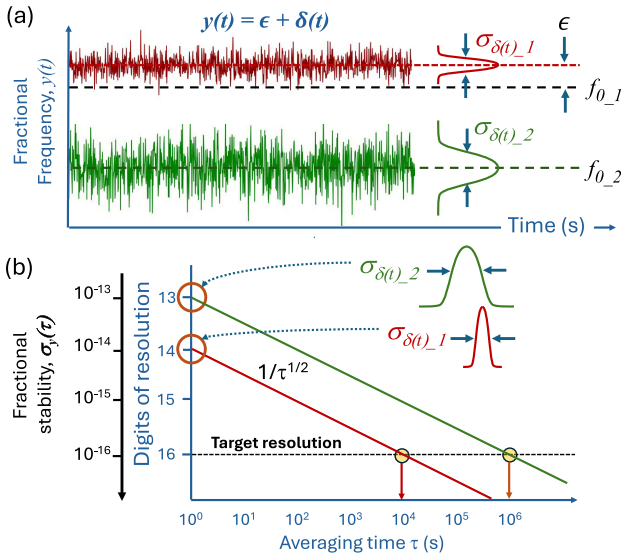

Fig. 4. Accuracy and instability in atomic clocks. (a) The accuracy refers to how much the mean clock output $y(t)$ differs from the unperturbed atomic frequency f_0, while fractional frequency instability relates to the statistical spread of $y(t)$. This spread can be quantified by the standard deviation of the instantaneous frequency deviations, $\sigma_{\delta(t)}$. Shown are two clocks: one more stable but inaccurate (red), and one more accurate but less stable (green). (b) The measured clock instability, expressed as the Allan deviation $\sigma_y(\tau)$, depends on the averaging period τ. Here, the higher instability of the green clock in (a) leads to a longer averaging period to reach a given resolution compared to the red clock. For white frequency noise, typical of atomic clocks when successive measurements are uncorrelated, the resolution improves as $\tau^{-1/2}$.

C. Choosing an Optical Reference Transition

When selecting transitions for highly stable and accurate atomic clocks, several factors must be considered

1. To achieve good short-term stability, the transition should have a narrow linewidth or long-lived upper state lifetime, and its frequency should be as high as possible (consistent with being accessible using available laser technology). This maximizes the Q-factor of the atomic reference.
2. To achieve good long-term stability and high accuracy, the clock transition should be minimally sensitive to external perturbations. This can be achieved by selecting atomic transitions that are naturally insensitive to environmental shifts because of fundamental symmetries.
3. Finally, the clock must be practical to operate. Ideally, the wavelengths needed for cooling, trapping, and clock spectroscopy should match commercially available laser sources.

However, there is no ideal system that meets all these criteria simultaneously. As a consequence, the development landscape for optical clocks features a multitude of species. Systems that have exceeded the performance of the present cesium primary frequency standard technology can be grouped into two broad categories: trapped-ion optical clocks and neutral-atom optical clocks. Further details are provided in Section 4. However as already indicated in Fig. 2, both neutral-atom and single-ion optical clocks

have seen amazing progress since the 1990s, with gains of seven orders of magnitude in three decades and further improvements still anticipated.

3. OPTICAL CLOCK OPERATION: AN ART OF PURITY AND CONTROL

High-performance optical atomic clocks operate in cycles that begin with cooling and trapping the atoms and conclude with measurement, or interrogation, of the transition frequency (Fig. 5).

A. Laser Cooling and Trapping

Laser cooling of the atomic sample is a critical step in optical clock operation because it reduces Doppler-induced frequency broadening and shifts, as well as collisions that can disrupt the coherence of the atomic state. It was first proposed in 1975 [29,30] and soon realized for both trapped ions [31,32] and neutral atoms [33]. Doppler laser cooling relies on momentum exchange between atoms and photons from a laser beam that is detuned slightly below the resonance frequency of an atomic transition. Atoms preferentially absorb photons that are counter-propagating to their motion, and subsequently emit those photons in a random direction. This results in a net momentum transfer which reduces the component of the atom velocity along the laser beam direction. Repeated absorption and re-emission of photons eventually leads to a steady-state temperature known as the Doppler cooling limit,

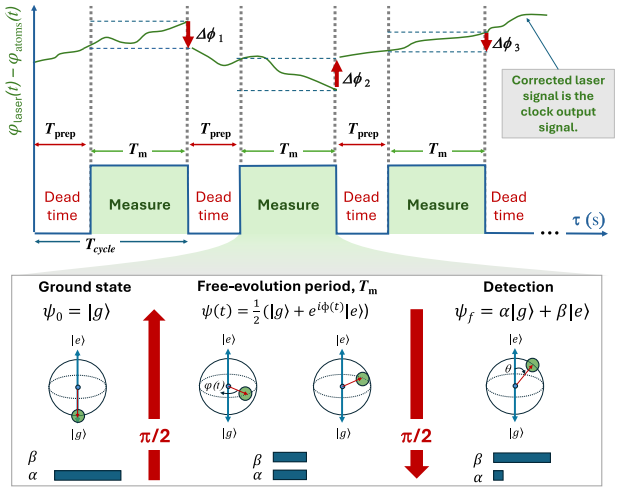

Fig. 5. Atomic clock cycle using Ramsey spectroscopy. At the top of the figure, we depict how sequential cycles are used to estimate the average frequency difference between the laser and the atomic transition. Each cycle begins with dead time, T_{prep}, during which the atomic sample is cooled, trapped, and prepared in a pure ground state. This is followed by a Ramsey phase, where we apply two $\pi/2$ pulses (laser pulses tailored in duration and amplitude to produce a $\pi/2$ rotation on the Bloch sphere) separated by a free-evolution period, T_m. This pulse sequence drives a coherent population transfer from an initial state, ψ_0, to a final state, ψ_f, as illustrated using the Bloch sphere (bottom inset). The first $\pi/2$ pulse initiates a superposition of the ground $|g\rangle$ and excited $|e\rangle$ states in a well-defined phase, which is then free to evolve during the period T_m. The second $\pi/2$ pulse has the effect of transforming the accumulated phase difference, $\Delta\phi_i$, between the superposition and the laser fields into a population difference of the excited and ground states. This population difference is then measured during the final phase of the clock cycle, enabling a frequency correction, $\Delta f_i = \Delta\phi_i / T_m$, that can be used to correct the clock laser to match the atomic transition frequency at the end of each cycle.

$T_D = \hbar\Gamma/2k$, where $\hbar$ and k are the reduced Planck constant and the Boltzmann constant, respectively, and Γ is the linewidth of the transition used for cooling.

The transitions typically used for the initial stage of laser cooling in optical clocks have linewidths of order 10 MHz, resulting in a Doppler cooling limit of around 1 millikelvin. While sufficient for high-accuracy operation of trapped-ion optical clocks, lower temperatures are required to achieve high efficiency loading of atoms from a magneto-optical trap (MOT) into an optical lattice (Section 4.B). A second Doppler cooling stage is therefore used in optical lattice clocks and employs a narrower linewidth transition to achieve temperatures in the microkelvin range.

Ions can be confined at relatively high kinetic energies and cooled within the trap, while in neutral-atom clocks cooling is an essential prerequisite for trapping. To achieve optimal performance, optical clocks are operated in the Lamb–Dicke regime, where the atomic motion is constrained to a region of dimensions small relative to the wavelength of the probing light [34]. This tight confinement results in discrete, quantized motional states.

The depth of the trap, in conjunction with cooling, is crucial for achieving the Lamb–Dicke regime. A deeper trap more effectively restricts the atom's motion, resulting in a larger energy gap between the trap's motional states ($n = 0$, $n = 1$, $n = 2$, etc.). Consequently, even if the measurement process causes an energetic recoil that excites the atoms to higher motional states, the ground-state transition can still be distinctly resolved from the excited motional states.

B. State Preparation and Measurement

Once cooled and trapped, the atoms' internal states are prepared, and the stable local oscillator is measured against the clock transition frequency. In ion clocks, a "repumping" laser is often used to return atoms from the excited clock state to the ground state via a short-lived intermediate level, thereby maximizing the signal strength via the number of atoms available for repeated interrogation.

A commonly used interferometric method for measurement of the clock laser with respect to the atomic transition is Ramsey spectroscopy [35]. We use this technique here to explain the concept of clock measurement and to explore the technical and quantum limits to clock measurement.

In Ramsey spectroscopy, a resonant laser pulse, known as a $\pi/2$ pulse, is applied to drive the atom halfway from the ground state to the excited state, creating an equal superposition of the two:

$$\psi(t) = \frac{1}{\sqrt{2}}(|g\rangle + e^{i\phi(t)}|e\rangle).$$

In Fig. 5, the Bloch sphere offers a geometric representation of the quantum state of the atom's two-level system. Here, the wavefunction's state vector, $\psi(t)$, is depicted as a point on the surface of a sphere, with the North and South poles representing the ground and excited states, and the surface describing all possible superpositions of these states. A $\pi/2$ pulse will result in a 90° rotation of the state vector about some axis, e.g., in the case of an atom initially in the ground state, such a $\pi/2$ will land the state vector on the equator.

After the first pulse, the atom evolves freely for a predetermined time, T_m, accumulating phase due to the detuning between the laser frequency and the atomic transition frequency,

$\Delta\phi = 2\pi(\nu_{\text{laser}} - \nu_{\text{atom}})T_{\text{m}}$. A second applied $\pi/2$ pulse then maps the accumulated phase difference ($\Delta\phi$) into a population difference between the ground and excited states.

This population difference is then typically measured via state-dependent fluorescence. A detection laser induces fluorescence only if the atom is in the ground state, while atoms in the excited state remain dark. By detecting this fluorescence (or its absence) to determine the atomic state, the phase evolution is disrupted, "collapsing" the superposition state. This forms the basis of an interferometric error signal used to correct the laser, keeping it frequency locked to the atomic resonance. In neutral-atom lattice clocks, many atoms are interrogated simultaneously, so the relative phase between the atoms and the laser can be estimated from the population distribution obtained in a single interrogation cycle. Because the projection noise scales as $1/\sqrt{N_a}$, these clocks obtain high phase sensitivity per cycle. In single-ion clocks, by contrast, only one atom is interrogated at a time, yielding a single binary outcome per cycle. The same $N_a^{-1/2}$ scaling applies to single ions, but with $N_a = 1$ each cycle, so statistical averaging must be built up over many repeated interrogations.

C. Measurement Noise Limits

Although accuracy often receives the most attention outside the clock community, it is the frequency instability, set by quantum and technical noise, that determines how long a clock must be average to reach a target resolution. Improved instability through the reduction of technical and quantum noise reduces the averaging time required to reach a target resolution, lowering the demands placed on clock robustness and operational effort.

One may conceptually distinguish between two limiting cases for estimating a clock frequency. In an idealized scenario, one could imagine a single Ramsey interrogation extending for the entire observation time τ, yielding a single-shot frequency sensitivity that scales as $1/\tau$. In practice, however, the free-evolution time T_{m} is limited by decoherence of the atomic superposition, so clocks operate in the regime $\tau \gg T_{\text{m}}$ and rely on many independent, statistically uncorrelated interrogation cycles. In this regime, the instability averages down as $1/\sqrt{T_m \tau}$, leading to the QPN expression:

$$\sigma_y(\tau) = \frac{1}{2\pi\,\nu_0\sqrt{N_a\,T_{\text{m}}\,\tau}}. \tag{1}$$

This equation gives the quantum projection noise (QPN)-limited frequency instability for Ramsey interrogation, where the characteristic $1/\sqrt{N_a}$ scaling defines the standard quantum limit (SQL) for uncorrelated atoms. If quantum correlations such as entanglement are introduced, the scaling can reach the Heisenberg limit, which scales as $1/N_a$ [36].

As seen in Fig. 6, increasing T_{m} substantially reduces the averaging time required to reach a target fractional-frequency instability for a given application. This improvement arises because a longer free-evolution time allows more phase to accumulate coherently during each Ramsey interrogation cycle, lowering the QPN-limited instability by a factor $1/\sqrt{T_{\text{m}}}$. In practice, however, T_{m} is often limited by technical decoherence of the atomic superposition to times far shorter than the natural lifetime of the clock transition. Laser drift and integrated phase noise from the cavity-stabilized probe laser typically restrict coherence times to below ~0.5 s, while magnetic-field and trapping-field inhomogeneities usually limit T_{m} to well under 1 s, despite the intrinsically long natural lifetimes of optical clock transitions.

These limitations raise the question of how optical clocks can still achieve uncertainties below 2×10^{-18} when the cavity-stabilized lasers used to interrogate the atoms typically exhibit fractional instabilities at the 10^{-16} level (see Section 5.A). The key point is that the laser does not set the long-term accuracy of the clock. It need only provide short-term coherence over the interrogation time T_{m}. The atoms, by contrast, serve as the long-term frequency reference: each Ramsey measurement yields the phase difference between the laser and the atoms, allowing the feedback loop to correct the laser's drift from one cycle to the next. Through

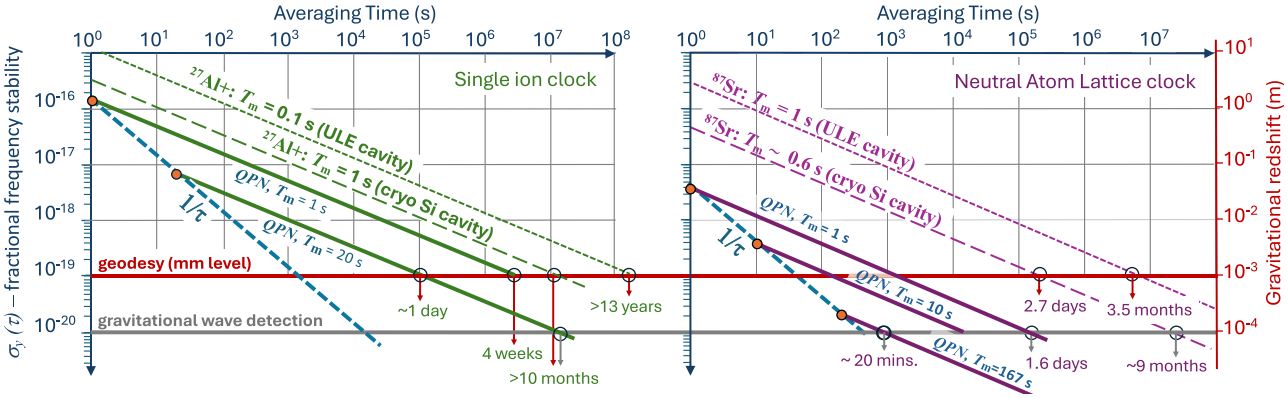

Fig. 6. Comparison of representative clock instabilities with the quantum-projection-noise (QPN) limits for a single-ion clock (left) and a neutral-atom lattice clock (right). Both plots share the same vertical axes on the left (fractional instability) and on the right (equivalent gravitational redshift). Left plot: solid green lines show the QPN-limited instability for a single ion clock ($N_a = 1$, $\nu_0 = 1.12$ PHz) for several interrogation times T_{m}, including the 20 s upper-state lifetime of the $^{27}Al^+$ clock transition. The dashed green lines show the extrapolated representative experimental instability with the clock operated with a room-temperature ULE [37] and cryogenic silicon cavity [23] with indicated T_{m}. The dashed blue line indicates the coherent single-shot sensitivity applicable only for $\tau < T_{\text{m}}$. The secondary right axis maps fractional instability to equivalent gravitational-redshift sensitivity. Right plot: solid purple lines show the QPN limits for a neutral-atom ^{87}Sr lattice clock ($N_a \sim 10^4$, $\nu_0 = 429$ THz), including the 167 s clock-state lifetime. Dashed purple curves show extrapolated representative measured instabilities for Sr clocks operated with duty cycle $\eta \sim 0.5$, using a ULE-cavity-stabilized laser ($T_{\text{m}} = 1$ s; [38]) and, for comparison, a cryogenic silicon–cavity-stabilized laser ($T_{\text{m}} \approx 0.6$ s; [39]). The red and grey horizontal lines crossing in both plots indicate averaging-time benchmarks relevant to key applications—e.g., millimeter-level relativistic geodesy and gravitational-wave background searches—determined by the intersections of desired fractional sensitivities with the plotted instabilities.

repeated interrogations, the laser's residual frequency noise is averaged down and its drift is removed, so that the clock output ultimately reflects the stability and accuracy of the atomic transition rather than that of the cavity-stabilized laser. This distinction also motivates the need to understand technical noise introduced by the measurement cycle itself, most notably the effect, which we discuss next.

Dead time between interrogation cycles, required for laser cooling and state preparation, reduces the duty cycle, $\eta = T_{\mathrm{m}}/(T_{\mathrm{m}} + T_{\mathrm{prep}}) < 1$, and prevents the QPN limit from being reached. In addition to degrading Eq. (1) by $1/\sqrt{\eta}$, dead time causes clock-laser frequency noise to alias onto the measured instability [40]. This arises because the sampling of the atomic signal imposes a square-wave-like sensitivity function whose Fourier components down-convert laser phase noise at harmonics of the cycle rate. In a simplified picture where the aliased probe-laser noise is treated as white phase noise and only the lowest-order harmonic is considered, the Dick-effect contribution to the Allan deviation can be approximated to scale as

$$\sigma_y(\tau)_{\mathrm{DE}} \sim \frac{1}{2\pi\nu_0}\sqrt{\frac{S_\phi(f_{\mathrm{cycle}})}{\eta\tau}}, \tag{2}$$

where $S_\phi(f)$ is the laser phase-noise spectral density and $S_\phi(f_{\mathrm{cycle}})$ denotes its value evaluated at the cycle frequency $f_{\mathrm{cycle}} \simeq 1/T_{\mathrm{cycle}}$ (see Fig. 5). This contribution, known as the **Dick effect** [41], is a technical instability arising from probe-laser noise rather than atomic projection noise. It is particularly impactful in optical lattice clocks, where the lower QPN limit makes laser technical noise and the Dick effect more prominent (see Fig. 6). Mitigation therefore requires high spectral purity of the probe laser, as discussed in Section 5.A.

D. Controlling and Evaluating Perturbative Effects

The accuracy of an optical atomic clock is ultimately limited by uncertainties in quantifying frequency shifts caused by residual interactions with fields. Achieving state-of-the-art accuracy requires precise control over the conditions under which the atoms are prepared and interrogated, in order to minimize perturbations to their internal energy levels.

Some of the most important effects arise from electromagnetic fields. In some cases, these fields are present because they are essential for controlling and measuring the atomic state, but it is also necessary to consider imperfectly shielded stray fields. Both magnetic fields (causing Zeeman shifts) and electric fields (causing Stark shifts) must be considered. This includes the blackbody radiation (BBR) shift, which is a quadratic Stark shift arising from the thermal radiation near 10 μm emitted by the apparatus surrounding the atomic sample. To account for their effect on the transition frequency, these unavoidable fields must be carefully modeled and measured. In some cases, continuous monitoring and feedback systems are also used to help stabilize time-varying shifts and hence improve the clock stability.

Relativistic effects that must be taken into account include not only the Doppler shifts arising from residual motion of the atoms relative to the probing lasers but also (when comparing clocks) the relativistic redshift that depends on position in the Earth's gravity potential (Section 7.B). Finally, even technical details like small errors in the control systems (servo systems) can introduce bias and must be carefully accounted for [38]. These will be highly dependent on the specific configuration of each apparatus.

Once an operator has carefully evaluated and corrected for all known perturbative effects, these are tabulated in the uncertainty budget for the clock. Assuming that the various contributions are uncorrelated, the uncertainties $\delta\nu_{\mathrm{shift}_i}$ can be combined in quadrature to determine the estimated fractional uncertainty of the clock:

$$\frac{\delta\nu}{\nu} = \frac{\sqrt{\sum(\delta\nu_{\mathrm{shift}_i})^2}}{\nu_{\mathrm{unperturbed}}}. \tag{3}$$

To validate these uncertainty budgets, comparison of independently developed clocks is essential (Section 6).

4. TYPES OF OPTICAL CLOCK

In pushing the frontiers of optical atomic clocks—for improved performance, broader applications, and tests of fundamental physics—physicists have advanced on multiple fronts simultaneously, striving for greater control over systematic effects and enhanced frequency stability.

Different optical clock architectures contribute uniquely to this progress. Single-ion clocks, $N_a = 1$ (Section 4.A), typically excel in accuracy due to minimal motional effects and strong isolation from environmental perturbations. On the other hand, optical lattice clocks (Section 4.B) leverage large ensembles of neutral atoms, $N_a \sim 10^4$, to reduce statistical uncertainties, making them especially powerful for achieving high short-term stability. Figure 7 summarizes the operation, challenges, and opportunities of these two clock architectures.

Pushing the boundary further (Section 4.C), nuclear clocks represent an emerging class of frequency standards operating at even higher transition frequencies, $\nu_{\mathrm{clock}} \sim 2$ PHz. Because their reference transitions occur within the nucleus—shielded from external electromagnetic fields by the surrounding electron cloud, they offer improved immunity against environmental shifts and potential for fractional accuracy at the 10^{-19} level.

A. Trapped-Ion Optical Clocks

The proposal that frequency references based on optical transitions in single laser-cooled trapped ions could reach fractional resolution of 10^{-18} dates back to the mid-1970s [29,42,43]. Ion traps for single ions employ an oscillating quadrupolar RF field, typically in the MHz range, to create an effective potential well that confines the ion in all three dimensions [14] and enables stable trapping for months at a time. This provides a nearly ideal environment for precision spectroscopy (Section 4.A.1). The clock transition is typically detected using the electron shelving technique [44], where the ion's fluorescence, which is normally observed during laser cooling, turns off when the ion is excited to the long-lived upper state of the clock transition. This change in fluorescence acts as a clear signal that the clock transition has occurred. However, the quantum projection limit to stability given by Eq. (1) is relatively high because only a single atom is used. To address this limitation, optical clocks based on ion crystals in linear ion traps [45] are being pursued (Section 4.A.2).

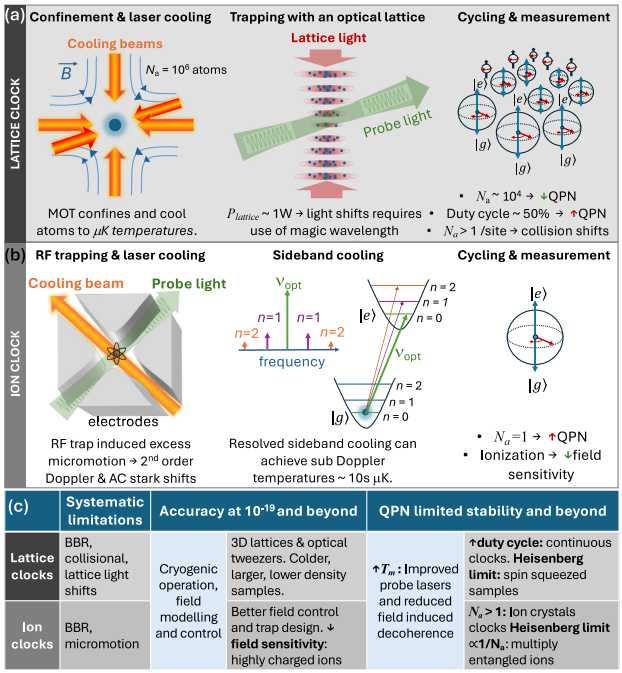

(c)	Systematic limitations	Accuracy at 10^{-19} and beyond		QPN limited stability and beyond	
Lattice clocks	BBR, collisional, lattice light shifts	Cryogenic operation, field modelling and control	3D lattices & optical tweezers. Colder, larger, lower density samples.	↑T_a: Improved probe lasers and reduced field induced decoherence	↑duty cycle: continuous clocks. **Heisenberg limit:** spin squeezed samples
Ion clocks	BBR, micromotion		Better field control and trap design. ↓ **field sensitivity:** highly charged ions		N_a > 1: Ion crystals clocks **Heisenberg limit** ∝1/N_a: multiply entangled ions

Fig. 7. Illustration of single-ion and neutral-atom lattice clock systems. (a) Neutral-atom lattice clock: magneto-optical trap (MOT) (left), 1D optical lattice (middle), and ensemble of Bloch spheres (right) depicting collective measurement behavior. (b) Single-ion clock: basic RF trap (left), sideband cooling (middle), and a Bloch sphere (right) representing quantum state evolution during measurement. (c) Current systematic limits, targeted goals and enabling approaches are listed by clock type.

1. *Single-Ion Clocks*

Single-ion optical clocks have been demonstrated in many species over the past four decades. A first major class is based on electric-quadrupole (E2) transitions between the $^2S_{1/2}$ ground state and a metastable $^2D_{5/2}$ or $^2D_{3/2}$ state in ions with alkali-like electronic structure. Examples include $^{40}Ca^+$ [46–51] $^{88}Sr^+$ $^{171}Yb^+$ $^{199}Hg^+$ $^{138}Ba^+$. These E2 transitions have natural linewidths of 0.2–3 Hz, corresponding to Q-factors of order 10^{15}, with $^{138}Ba^+$ standing out as an unusually narrow E2 system at 2 mHz.

A second class is represented by the electric-octupole (E3) transition in $^{171}Yb^+$. This highly forbidden $^2S_{1/2} - {}^2F_{7/2}$ transition has a natural linewidth near 1 nHz [52], enabling very long interrogation times, although the usable duration is ultimately limited by the probe-laser coherence.

A third class consists of ions with two valence electrons, analogous to neutral alkaline-earth atoms, including $^{115}In^+$ [53–55] $^{27}Al^+$, and $^{176}Lu^+$. The clock transitions in $^{115}In^+$ and $^{27}Al^+$ are the spin-forbidden $^1S_0 - {}^3P_0$ lines, with natural linewidths of 0.8 Hz and 8 mHz, respectively. The $^{176}Lu^+$ ion offers three possible clock transitions, with current work focusing on the $^1S_0 - {}^3D_1$ line.

A single laser-cooled trapped ion behaves nearly as a stationary, isolated quantum system, ideal for high-resolution spectroscopy. With low background gas pressure and cooling into the Lamb–Dicke regime, collisional and Doppler effects are strongly suppressed. Because the ion remains trapped for indefinite durations, a high duty cycle can be maintained. However, interaction with the trapping fields and residual motion introduce systematic shifts that must be carefully controlled to reach the highest accuracies.

Within the ion trap, any mechanism that acts to displace the ion from the trap center induces residual interaction with the trapping field that results in a Stark shift of the clock transition frequency. **Motionally induced frequency shifts** must also be carefully controlled, with both residual thermal motion (slow secular motion) and motion induced by the trap drive frequency itself (faster micromotion) needing to be considered. The linear Doppler effect from secular and micromotion leads to sidebands in the optical spectra, but does not shift the optical carrier; however, a second-order relativistic Doppler shift must be considered. Because micromotion results in faster displacement, it results in larger Doppler shifts with higher additive uncertainty at levels close to 1 part in 10^{17} if not carefully controlled. Methods must therefore be employed to measure this micromotion, e.g., by observing modulation of the cooling laser fluorescence at the trap drive frequency [56], and to minimize it by applying voltages to dc compensation electrodes.

If the trap motional sidebands can be frequency resolved, a technique called resolved sideband cooling can also be used to localize the atomic sample into the motional ground state (Fig. 7), enabling clocks to achieve sub-Doppler temperatures. Sideband cooling selectively removes energy from the atoms by using laser light tuned to the lower motional sideband of the atomic transition frequency [57]. In this case, the laser is red-detuned from the carrier frequency by one quantum of the trap's motional frequency, which reduces the atom's motional state by one quantum at a time until it reaches the motional ground state, $n = 0$ [58].

In some ion clocks, such as those based on $^{88}Sr^+$, $^{171}Yb^+$, and $^{40}Ca^+$, a significant contribution to the uncertainty comes from the interaction between any electric field gradient experienced by the ion and the non-spherical charge distribution of the upper state of the clock transition (electric quadrupole moment). The size of this shift depends on the magnitude of the field gradient, its orientation with respect to the magnetic field, and the quadrupole moment of the specific atomic state involved. Typically, this effect is averaged out by making measurements in three orthogonal magnetic field orientations [59] or an appropriate set of magnetic sublevels [60]. In other ion clocks, such as $^{27}Al^+$ and $^{115}In^+$, there is negligible quadrupole shift of the clock transition because neither atomic state has an electric quadrupole moment.

Both $^{27}Al^+$ and $^{115}In^+$ exhibit low blackbody radiation shift. However, ultraviolet laser sources are required for cooling and probing the ion, which presents an experimental challenge. In the case of $^{27}Al^+$, the ion is sympathetically cooled by an auxiliary ion of a different species that can be cooled at a more convenient wavelength and quantum logic spectroscopy techniques [61] are used to map the clock transition information back to the auxiliary ion for readout. Sympathetic cooling is also used in recent implementations of $^{115}In^+$ single ion clocks [62], but in this case a suitable transition exists for direct state detection, reducing experimental complexity.

The lowest uncertainty reported to date for a trapped-ion optical clock is 5.5×10^{-19}, for the NIST $^{27}Al^+$ clock [23], with a second independent realization of this system at Huazhong University of Science and Technology (HUST) having an evaluated uncertainty of 1.6×10^{-18} [63]. Several other trapped-ion clocks, including $^{171}Yb^+$ E3 [64–67] $^{115}In^{+40}$ and Ca^+, have also reached estimated systematic uncertainties in the low 10^{-18} range.

However, the criterion set in the roadmap for redefinition of the second is that three independent optical frequency standards based on the same reference transition should have published uncertainty budgets at the 2×10^{-18} level or better [24]. This criterion has not yet been met by any trapped-ion optical clock.

2. Ion Crystal Clocks

The stability of single-ion clocks is fundamentally limited by the low signal-to-noise ratio of a single ion (Section 3.C). Ion crystal clocks aim to overcome this limitation through simultaneous interrogation of N_a atoms in a Coulomb crystal, reducing the time necessary to achieve a given frequency resolution by a factor of N_a compared to the single ion case. The challenge, however, is to achieve the necessary level of control over systematic frequency shifts.

In particular, in linear ion traps the Coulomb fields of neighboring ions in the crystal result in the clock ions experiencing significant electric field gradients [45]. This limits the choice of suitable ions for such a clock to those for which neither state of the reference transition has an electric quadrupole moment, as for other species the electric quadrupole shift would be unacceptably large and difficult to control at the necessary level. Examples of suitable reference transitions are the $^1S_0-{}^3P_0$ transitions in two-electron systems such as $^{115}In^+$ and $^{27}Al^+$.

The first ion crystal clock was realized recently, using a setup in which $^{115}In^+$ clock ions are trapped together with $^{172}Yb^+$ ions which are used for sympathetic cooling [66]. For the initial evaluation of this clock, a four-ion Coulomb crystal was used, consisting of a single $^{115}In^+$ ion and three $^{172}Yb^+$ ions. In this system, the overall fractional systematic uncertainty was assessed to be 2.5×10^{-18}.

Frequency ratio measurements were also performed relative to the optical clock transitions in ^{87}Sr and $^{171}Yb^+$ (E3), with relative uncertainties of 4.2×10^{-17} and 4.4×10^{-18}, respectively. Impressively, for a new clock entering the field, the latter is the most precisely measured optical frequency ratio reported in the published literature to date. A first step toward operation with multiple clock ions was also demonstrated by making stability measurements against the $^{171}Yb^+$ (E3) optical clock. The stability at 1 s averaging time was observed to improve from 1.6×10^{-15} for a single clock ion to 9.2×10^{-16} for four clock ions. This is lower than the expected improvement factor due to ion-number-dependent dead time in the state preparation phase, but a strategy is in place to reduce this dead time in the future using an additional laser source in the measurement setup. Ion trap arrays of the type used in this demonstration have separately been shown to support optical clock operation with approximately 100 ions while achieving accuracies better than 10^{-18} [68].

Optical clocks based on three-dimensional Coulomb crystals of around 1000 ions have also been proposed [69,70], with the potential for achieving even more significant gains in measurement signal-to-noise and hence frequency stability. Although more ions translate to the possibility of higher systematic shifts due to ion-ion interactions and motional effects, references [69,70] indicate that accuracies of 10^{-19} are feasible.

B. Neutral-Atom Optical Lattice Clocks

Neutral atoms exhibit much weaker long-range interactions than ions, allowing them to be operated in large ensembles and thereby achieving significantly better signal-to-noise, and hence improved measurement stability, than single-ion clocks. While RF traps naturally confine laser-cooled ions within the Lamb–Dicke regime, the magneto-optical traps (MOTs) used to cool neutral atoms do not. To achieve Lamb–Dicke confinement for neutral atoms, 1D optical lattices are employed, formed by counter-propagating laser beams that create pancake-shaped trapping potentials, typically holding 10 to 20 atoms per site [71]. However, the high light intensities required to form these lattices induce substantial AC Stark shifts of the clock transition frequency. The key breakthrough in optical lattice clocks was the proposal of a "magic wavelength"—a lattice laser frequency at which the AC Stark shifts of the ground and excited clock states are equal, canceling the net shift of the clock transition [72].

Optical lattice clocks operate on the ultra-narrow $^1S_0-{}^3P_0$ transition in alkaline-earth(-like) atoms. In fermionic isotopes, this transition is weakly allowed due to hyperfine mixing from nonzero nuclear spin, yielding millihertz-level linewidths ideal for precision. Spin-polarized fermions also benefit from suppressed s-wave collisions, reducing collisional shifts.

In bosonic isotopes, which lack nuclear spin, the transition is strictly forbidden and must be enabled by magnetic-field-induced mixing between $^3P_1$ and $^3P_0$. These systems are generally more sensitive to collisional shifts, though lattice clocks based on bosons such as ^{88}Sr [73,74] ^{174}Yb have been demonstrated. The most widely used systems today remain ^{87}Sr [75] and ^{171}Yb.

The lowest reported uncertainty to date for an optical lattice clock is 8.1×10^{-19}, for the 1D ^{87}Sr optical lattice clock at JILA [22]. Only one other optical lattice clock (^{171}Yb at NIST [76]) has reached the target uncertainty of 2×10^{-18} set in the roadmap for redefinition of the second, although uncertainties below 5×10^{-18} have been reported for two other ^{87}Sr clocks [77,78].

A key systematic limitation for both ^{87}Sr and ^{171}Yb is the **BBR shift** (Section 3.D), which induces frequency shifts at the hertz level, corresponding to parts in 10^{-15}. Operating clocks at cryogenic temperatures can suppress this shift [79,80], though at the cost of significant added complexity. An alternative room-temperature strategy for reducing BBR-related uncertainty is to use clock transitions at higher frequencies, such as in the UV, where room-temperature thermal photons are further off-resonance. This makes species like ^{199}Hg particularly favorable [81,82]. Other experimentally investigated candidates with intrinsically low BBR shifts include Mg [83], Tm [84], and Cd [85].

The high atomic densities in optical lattice clocks mean that **density-dependent frequency shifts** must also be carefully evaluated. In bosonic isotopes, such as ^{88}Sr, atoms readily collide in a way that shifts the clock frequency, requiring either low densities or careful calibration to correct for these effects. In fermionic isotopes, such as ^{87}Sr, the Pauli exclusion principle suppresses collisional interactions when atoms share the same internal state. However, at ultracold temperatures, p-wave interactions still contribute to frequency shifts. One mitigation strategy involves adjusting the excitation fraction, allowing collisional shifts from ground- and excited-state atoms to partially cancel [86]. Alternatively, atoms can be confined in a 3D lattice to ensure single occupancy per site, effectively eliminating collisions [87]. Despite its advantages, the 3D approach introduces added complexity and potential systematics from heating and lattice imperfections, so most optical lattice clocks currently operate in a 1D lattice configuration.

Lattice light shifts depend on how accurately the magic wavelength can be realized in practice, and estimating the associated

uncertainty requires species-specific models [22,88]. Although reducing the lattice intensity can mitigate these shifts, it also lowers atom number and degrades the signal-to-noise ratio. To overcome this tradeoff, a technique known as Sisyphus cooling can be used to cool atoms below the Doppler limit. Because this enables the creation of colder, more dilute ensembles that can be loaded into shallower lattices with more occupied sites, it has the potential to simultaneously reduce collisional and lattice light shifts while supporting higher atom numbers for improved QPN-limited stability [89,90].

State-of-the-art optical lattice clocks have demonstrated better short-term frequency stability than trapped-ion clocks, owing to their larger number of atoms [39]. However, reaching the quantum projection noise limit [Eq. (1)] is hampered by the Dick effect (Section 3.C) that arises because of dead time between clock interrogation periods: one way to eliminate this additional source of noise is through interleaved interrogation of two cold-atom ensembles with a common probe laser [91]. In such an arrangement, provided that dead time can be reduced to 50% of the measurement cycle time, the stability achievable is dictated purely by the atomic ensemble. An alternative under development by the Katori group at the University of Tokyo and RIKEN [92] involves continuous interrogation using spatially separated ensembles in a conveyor-belt-like scheme [93].

C. Emerging Clock Technologies

Various other types of novel clock technology are being pursued in various laboratories around the world. These include active optical clocks to achieve high stability without the need for complex cavity-stabilized lasers [94,95] and optical tweezer clocks for improved control over atom–atom interactions [96], though such systems still have some way to go to achieve performance close to state-of-the-art. Another recent development is the first full evaluation of a highly charged ion clock [97], verifying control of systematic effects at the low parts in 10^{17} level, competitive with many other established optical clocks worldwide. Although far more complex than traditional trapped-ion clocks, and thus unlikely to be used for timekeeping, highly charged ion (HCI) clocks offer promising opportunities for testing fundamental physics (Section 8.A). Their increased charge states also broaden the accessible parameter space, potentially revealing new clock transitions that align with commercially available laser wavelengths. However, perhaps the most exciting advance of recent times is the first demonstration of a new type of "nuclear clock" based on thorium-229 [98–100].

1. Nuclear Clocks

The thorium-229 transition used as the reference for frequency stabilization of a laser oscillator is a radiative transition inside the nucleus rather than a transition within the electron shell. The unique feature of ^{229}Th is an exceptionally low-energy transition between the nuclear ground state and the first excited state (by far the lowest identified for any atomic nucleus). This falls within the optical photon energy range and hence is accessible to laser spectroscopy. Additionally, because nuclear transitions are deeply buried within the atomic structure, they are nearly perfectly immune to the field-induced Stark shifts that plague clocks based on electronic excitations. These characteristics led to a proposal in 2003 that the ^{229}Th transition could form the basis of a highly accurate clock [101].

However, the uncertainty in the transition energy was enormous (∼4 eV or 1 PHz), making experimental implementation a formidable challenge. Early nuclear spectroscopy estimates placed it at ∼3.5 eV, but later experiments revised this to more than twice that value [102]. It was not until 2024 that laser excitation of the transition was finally achieved [103], marking a key breakthrough that has rapidly advanced progress toward a nuclear clock.

One major challenge in realizing a thorium nuclear clock is the complexity of the laser system required to probe the transition. A recent milestone was the direct measurement of the frequency ratio between the ^{229}Th nuclear clock transition and a ^{87}Sr optical lattice clock, enabled by a vacuum ultraviolet (VUV) frequency comb [104]. This system bridges the visible and VUV domains using high-harmonic generation techniques developed in attosecond and high-field laser physics [105]. The process involves focusing ∼50 W into a xenon sample to generate the seventh harmonic of a stabilized frequency comb near 1 μm. Maintaining coherence in this highly nonlinear process is critical, as the generated laser light at 148 nm must have a comparable linewidth to the nuclear transition to achieve high-fidelity measurements.

The immunity of nuclear energy levels to perturbation by electromagnetic fields opens up a new possibility by using a crystal to hold the nuclei stationary rather than using an electromagnetic or optical trap. This would bring obvious benefits to improving the portability of nuclear clocks, though the VUV laser technology required remains a challenge in this respect. The systematic frequency shifts of the nuclear clock transition have yet to be studied in detail, though the breakthroughs of last year have brought a nuclear clock significantly closer to reality. For timekeeping applications, it remains an open question whether or not nuclear clocks will surpass the accuracy of optical clocks. However, they could also find other applications, such as precision measurements of nuclear structure, as well as other tests of fundamental physics (Section 8.A).

5. SUPPORTING OPTICAL TECHNOLOGIES

A. High-Performance Cavity-Stabilized Lasers

Optical atomic clocks rely on probing extremely narrow atomic transitions, often with natural linewidths in the millihertz range. Consequently, this demands a laser source with exceptionally low phase noise and high-frequency stability. Commercial single-frequency lasers typically exhibit 3 dB linewidths exceeding 10 kHz over 1 s timescales and suffer from significant frequency drift. As a result, active stabilization and spectral filtering are essential for optical clock spectroscopy, which requires the laser to remain phase-coherent with the atomic transition over the free-evolution time, T_m (Section 3.C). To address this, techniques were developed in the 1980s to lock lasers to high-finesse Fabry–Perot optical cavities [106], enabling sub-hertz linewidths [107] suitable for high-resolution optical spectroscopy and atomic clock interrogation.

As seen in Fig. 6, to date optical clock system stability is still limited by the probe laser noise and its drift, which can both constrain the maximum free evolution time. To improve local oscillator performance, optical cavities have been designed and housed to minimize the effect of environmental noise, including temperature

and pressure changes, and vibration and acoustic noise. With careful engineering, the length stability of an optical reference cavity can approach the thermomechanical noise floor set by Brownian motion in the cavity materials at finite temperature [108,109]. These sources of noise can be mitigated using high Young's modulus materials for spacers and mirrors to suppress thermal motion. In current state-of-the-art systems, the dominant contribution is Brownian noise in the mirror substrates.

Several techniques have been pursued to further reduce this limit to thermomechanical noise. For instance, high mechanical Q-factor mirror coatings have been shown to reduce Brownian motion at room temperature by an order of magnitude [110]. The average mirror thermal fluctuations can also be reduced by increasing the laser spot size on the cavity mirrors. Alternatively, longer optical cavities can be built to proportionally reduce the effect of length instabilities. Although this makes vibration isolation more challenging, the state-of-the-art fractional frequency instability reached for room temperature cavities (noise floor below 1×10^{-16}) was achieved using cavities almost 0.5 m long [111,112]. Finally, cavities can be operated at cryogenic temperatures. To date, two materials with near-zero thermal expansion at cryogenic temperatures have been explored: single-crystal silicon and sapphire. Single-crystal silicon cavities, operated at 124 K, have achieved state-of-the-art thermal noise-limited performance of 4×10^{-17} for integration times between 0.8 s and a few tens of seconds [113]. More recently, sapphire cavities operated at 10 K have been explored. While these offer the prospect of thermal-noise-limited fractional frequency instabilities in the 10^{-18} range, the best short-term stability achieved to date is 10^{-16} at 1-s averaging time [114].

B. Optical Frequency Combs

When optical references were first being developed a significant challenge loomed regarding how to measure their transition frequencies, which cycle 100,000 times faster than state-of-the-art electronics. Prior to the development of optical frequency combs, transition frequencies were measured using complex harmonic frequency chains that linked optical frequencies to the primary cesium standard at 9.2 GHz [115]. Due to their complexity, only a handful of absolute optical frequency measurements were published prior to the year 2000.

The optical frequency comb (OFC) represented a breakthrough in metrology because it could perform near-perfect optical-to-microwave down-conversion with a single oscillator, enabling the generation of microwave timing signals that could be counted using commercial frequency counters. An OFC (Fig. 8) is a mode-locked laser that uses frequency control techniques to transfer the stability of an atomic reference to its optical pulse train [116]. This control is achieved by stabilizing the pulse-to-pulse timing, as well as the absolute frequency and phase of the pulse optical carrier [116]. Stabilization, combined with coherent nonlinear broadening in optical fibers [117] and waveguides, enables the generation of octave-spanning spectra containing 10^5 to 10^6 discrete, extremely well defined, and equally spaced optical modes. Remarkably, phase-stabilized frequency combs have demonstrated pulse-to-pulse timing stability at sub-femtosecond levels, uncertainty in the optical mode spacing across an octave of bandwidth at the 10^{-20} level [118], and nanohertz-level frequency control in their optical modes [119]. Frequency combs were first demonstrated using Ti:sapphire lasers, which offered broad gain bandwidth for wide spectral coverage. They were soon extended to Er:doped and Yb:doped fiber lasers for improved robustness and to a variety of mode-locked laser platforms tailored to access different regions of the optical spectrum [120].

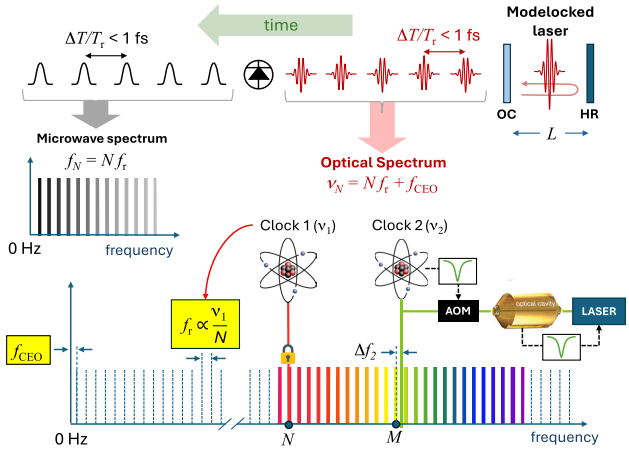

Fig. 8. Depiction of the operation of an optical frequency comb. A mode-locked laser, modeled as a two-mirror cavity with a high reflector (HR) and output coupler (OC), emits a train of femtosecond pulses. In the frequency domain, this corresponds to an optical frequency comb: a spectrum of equally spaced modes separated by the repetition rate f_r and offset by the carrier–envelope offset frequency f_{CEO}. Photodetection yields a microwave signal at $f_r = 1/T_r = c/2L$ at the cavity free-spectral range, with no sensitivity to f_{CEO}. The comb is stabilized by locking mode N to a reference laser at ν_1, so that $\nu_N = Nf_r + f_{CEO} = \nu_1$, transferring its stability to all comb modes. A second optical frequency ν_2 can be measured using nearby mode M, enabling precise frequency comparisons between widely separated optical references. Using the 2nd standard for illustration, a single-frequency laser, with frequency $\Delta\nu_2$, is stabilized to a resonant mode of a high-finesse optical cavity and then shifted into resonance with an atomic transition using an acousto-optic modulator (AOM).

In OFCs, the mode-locking mechanism establishes a deterministic and phase coherent relationship between all optical modes in the spectrum whereby each mode, ν_N, can be characterized by only two radio frequencies:

$$\nu_N = Nf_r + f_{CEO}. \tag{4}$$

Above, N is a large integer multiplier (typically on the order of 10^5–10^6) that scales the cavity resonant mode spacing or repetition rate, $f_r = c/2L$ into the optical domain. Here c is the speed of light and L is the optical cavity length. For a linear cavity of length $L = 30$ cm, $f_r = 500$ MHz. The carrier–envelope offset frequency f_{CEO} represents a common shift applied to all optical comb lines, defining their absolute frequencies and linking the optical comb spectrum to zero frequency.

Alternatively, ν_N can be stabilized by using the difference frequency, $\Delta\nu_1$, between an optical clock frequency, ν_1, and the nearest comb mode as an error signal for control of the OFC cavity length. As seen in Fig. 8, this transfers the optical reference stability via division to the microwave domain through f_r, and thus through Eq. (4), to all optical and microwave modes of the comb.

Optical-to-optical synthesis can be engineered with near-perfect fidelity [119]. In optical-to-microwave conversion, both frequency and noise scale with the reference, enabling the generation of signals over 1,000 times more stable than the best

room-temperature electronic oscillators [121–123], leading to the recent commercialization of photonic-based synthesizers.

Using the above stabilization process, frequency combs can enable the measurement of optical standards with respect to the hertz via frequency division. Additionally, OFCs enable the relative frequency comparison of multiple optical clocks through the measurement of frequency ratios. Because ratios are unitless, they are not limited by the 10^{-16} uncertainty of the hertz through the SI second. For example, if two clocks with frequencies ν_2 and ν_3 have beat frequencies and Δf_3 with modes M and K, respectively, the ratio is simply calculated as

$$\frac{\nu_3}{\nu_2} = \frac{K f_r + f_{CEO} + \Delta f_3}{M f_r + f_{CEO} + \Delta f_2}. \quad (5)$$

6. VALIDATING OPTICAL CLOCK PERFORMANCE

Optical atomic clock comparisons provide a critical test of clock accuracy and reliability. While uncertainty analyses represent each laboratory's best effort to account for all known frequency shifts—such as those from electromagnetic fields, motion, or environmental effects—they remain estimates until they are validated through experiment. Direct comparisons between independent optical clocks are essential to confirm that no significant systematic uncertainties have been overlooked or underestimated. These comparisons not only build confidence in the reported uncertainties and accuracy in reported frequencies, but also support international consistency in optical frequency standards.

A. Local Frequency Comparisons

As described in Section 5.B, frequency combs can compare the frequency of an optical clock to a local cesium primary frequency standard, enabling the absolute frequency of the optical clock to be determined in units of hertz. However the accuracy of the best such measurements [124,125] is limited to around 10^{-16} by the accuracy of today's primary standards. This limitation can be bypassed by comparing optical clocks directly.

The most straightforward type of comparison is between two optical clocks based on the same transition, co-located within the same institute, where the frequency ratio between the two clocks is expected to be unity. Several such comparisons have been performed, with the lowest uncertainties achieved being 1×10^{-18} for a comparison between two ^{171}Yb optical lattice clocks [76], 3.8×10^{-18} for a comparison between two $^{176}Lu^{+}$ optical clocks [126] and 4.2×10^{-18} for a comparison between two $^{171}Yb^{+}$ E3 ion optical clocks [127].

It is also possible to compare co-located clocks operating at different frequencies using an optical frequency comb (Section 5.B). In such cases, the frequency ratio is not known *a priori*, so validating the clocks' uncertainty budgets requires comparison with independent measurements from other laboratories. A key advantage is that this validation does not require a physical link as published frequency ratio results can be used instead. Although comparisons of this kind have been performed since the early 2000s, the first local measurement with fractional uncertainty below 5×10^{-18}—meeting the target for redefinition of the SI second—was only reported in 2025, between the $^{115}In^{+}$ and $^{171}Yb^{+}$ (E3) transitions [66] at PTB in Germany. However, no independent measurement of this ratio is yet available for cross-validation.

Efforts to directly connect independently developed optical clocks across global national metrology institutes aim to provide the most rigorous tests of uncertainty budgets. Such comparisons are far more challenging as they involve either remote comparison using long-distance links or transportable versions of the high-accuracy optical clocks. These comparisons are essential for validating optical clock uncertainties, as the redefinition roadmap requires agreement between independent clocks at the 5×10^{-18} or better [24].

B. Remote Frequency Comparisons

When using long-distance time and frequency links to compare geographically separated optical clocks, environmental perturbations, signal delays, and other sources of noise introduced during transmission must be carefully managed to ensure the integrity of the transferred time and frequency signals.

1. Microwave Time and Frequency Transfer Links

Microwave atomic clocks around the world are routinely compared via satellite-based microwave time-transfer links (GNSS and TWSTFT) to generate the global time scale UTC (Fig. 1). The transmitted signals are subjected to varying delays as they pass through the ionosphere and troposphere, and the effects of satellite motion must also be accounted for. Although the two-way configuration and the use of geostationary satellites reduce these effects in TWSTFT, long averaging periods are required to reach low link uncertainty (Fig. 9).

Microwave time-transfer links have been used to compare optical clocks by connecting them to hydrogen masers via optical frequency combs [135]. However, dead time in optical clock operation requires extrapolation to maintain phase coherence, introducing maser noise and additional uncertainty. Even with advanced carrier-phase techniques—such as GPS PPP [136], IPPP [137], TWCP [138], or higher-bandwidth modulation [139]—uncertainties remain at the low 10^{-16} level [135,138,139].

A recently developed method for optical clock comparison is very-long-baseline interferometry (VLBI), which uses geographically separated radio telescopes to observe the same celestial source, forming a virtual telescope with enhanced angular resolution. This requires the individual telescopes to be referenced to local atomic clocks in order to ensure precise correlation of the signals recorded in different locations. VLBI has been used to compare optical clocks in Italy and Japan using portable stations [140]. In these experiments, timing signals from extragalactic radio sources served a role similar to GNSS in remote clock comparisons. Although the achieved uncertainties were comparable to those of GNSS and TWSTFT links, VLBI demonstrated improved link stability—reaching 2×10^{-16} after one day of averaging—and could potentially reach the low 10^{-17} range after ten days [140].

In the near term, perhaps the most exciting prospects for using microwave links to compare optical clocks are opened up by the recent launch of the Atomic Clock Ensemble in Space (ACES) mission [141] to the International Space Station (ISS). Installed on the exterior of the Columbus module of the ISS, the mission features two cutting-edge microwave atomic clocks: Projet d'Horloge Atomique á Refroidissement d'Atomes en Orbite (PHARAO), a laser-cooled cesium atomic clock, and Space Hydrogen Maser (SHM), which are designed for long-term accuracy and short-term stability, respectively.

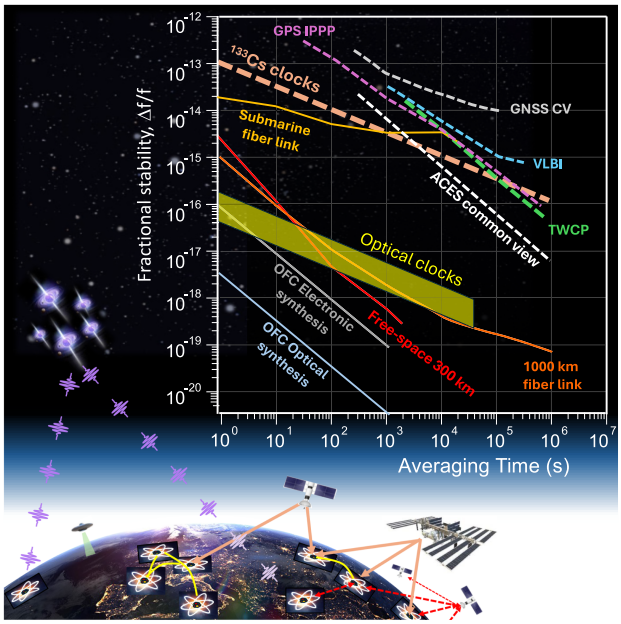

Fig. 9. Fractional-frequency stability of atomic clocks, optical and microwave transfer links, and photonic synthesis techniques for terrestrial and space-based networks. Dashed lines denote microwave systems; solid lines denote optical systems. Satellite-based microwave links include GPS integer precise point positioning (IPPP, pink dashed) [128], two-way carrier-phase transfer (TWCP, green dashed) [128], GNSS two frequency real-time common view (GNSS CV) (grey dashed) [129], and ACES (white dashed) [130]. Also depicted is the link noise due to VLBI comparisons (purple) [131]. In the optical domain, the link noise of ground-based optical fiber (orange) [132], submarine fiber [133] (light orange), and free-space links (red) [134] are compared. Also shown is a range of performances for state-of-the-art optical atomic clocks (yellow band) and the additive instabilities from optical frequency combs (OFC) used for the electronic synthesis (grey solid line) [123] and optical synthesis (blue solid line) [119] of atomic references needed for optical clock measurement. Note that the presented curves represent the best-case performance ranges from demonstrations in the literature. The achievable instabilities of all links depend strongly on baseline, post-processing, hardware calibration, and environmental conditions.

These space clocks will be compared to ground clocks using the ACES microwave link (MWL), a two-way link that operates in the Ku band (13.5 GHz for the uplink and 14.7 GHz for the downlink). The two-way configuration suppresses tropospheric and ionospheric time delays, with the high operating frequency being particularly advantageous for reduction of the ionospheric delay and also cancels the first-order Doppler effect. A third frequency in the S band (2.2 GHz, downlink only) is used to determine the ionosphere total electron content (TEC). Because the ISS is in low-Earth orbit, a ground station sees it for only about 300 s during each 90 min pass. To reconnect these short measurement intervals, the ACES system tags the microwave signal with a pseudo-noise (PN) code, which acts like a unique identifier that prevents phase ambiguity between passes. Microwave link ground terminals will be located in Europe, the US, and Japan, and up to four of these can be connected at once, distinguished by different Doppler shifts and PN-codes. In addition to space-to-ground comparisons, the MWL will therefore allow direct comparisons between ground clocks to be performed at a level of stability beyond what has been possible up till now. When the ISS is in common view of two ground stations (e.g., within Europe), the system should be able to achieve a comparison accuracy of 1 part in 10^{17} within a few days [142]. For intercontinental comparisons, where there is no period of common view, around one week is expected to be needed to reach this level.

However, the stability of even advanced microwave time-transfer links remains orders of magnitude worse than the stability of optical atomic clocks, and this motivates the pursuit of optical links to achieve higher resolution [143].

2. Optical Time and Frequency Transfer Links

Optical fiber is an attractive medium for comparison of time and frequency signals, as it is easier than open-air paths to protect from environmental perturbations, and extensive low-loss fiber infrastructure is already in place for optical communications systems. Building on bi-directional phase-noise cancelation approaches initially demonstrated on a 25 m link [144], fiber-based optical frequency transfer has been scaled to municipal [145–148] and intracontinental [149–151] scales.

Currently, Europe has one of the best developed and most extensive fiber networks for optical frequency comparison and dissemination, linking national metrology laboratories across France, Germany, the UK, and Italy, as well as other research institutes. These fiber links enable relative atomic clock measurements and the dissemination of stable optical and microwave signals with additive inaccuracies on optical signals as low as 1 part in 10^{19}. These levels of resolution have been achieved over links of nearly 1000 km within less than a day of averaging [152]. Hence, clock comparisons over optical fiber [149,153] are limited by the performance of the optical clocks themselves rather than that of the link (Fig. 9).

Connecting optical clocks in different continents via optical fiber presents additional challenges, since this will normally require a submarine link. On land-based frequency transfer links, the standard unidirectional amplifiers used in telecommunications are replaced by bidirectional amplifiers, but this is not feasible for a submarine link, and so two separate fibers have to be used rather than a fully bidirectional link. The degree to which it is possible to compensate for environmentally induced fiber noise will therefore depend on the degree of noise correlation between the two fibers. Nevertheless based on initial studies of frequency transfer over submarine telecommunications links, it seems possible that intercontinental clock comparisons could be achieved at a similar level to satellite-based techniques, but with averaging times around 100 times shorter [133].

Many laboratories developing optical clocks lack access to metrological grade optical fiber links and are highly geographically dispersed. Free-space optical time-transfer links are therefore also being pursued to address the gap in ability to perform high-precision clock comparisons on a global scale.

Free-space optical frequency transfer using a continuous-wave (CW) optical carrier, as with fiber links, has been demonstrated [154]. However, signal dropouts due to atmospheric turbulence limit the time for which coherent operation can be maintained, because the period of the optical carrier is too short to avoid cycle slips after these dropouts. Phase coherence for more than 1 h has been demonstrated over sub-kilometer links through the use of adaptive optics [155], but an alternative is to use pulsed radiation.

For example, in addition to the MWL, the ACES mission also includes an optical link: European Laser Timing (ELT) [141]. This is an extension of the former T2L2 time transfer experiment on board the Jason-2 satellite [156] based on satellite laser ranging

with picosecond laser pulses. Ground-based tests suggest that this should have performance similar to the MWL and thus will act as an important cross-check for that link.

Higher timing accuracy can be achieved using frequency-comb-based optical two-way time and frequency transfer, with OFC laser terminals at both ends of the link. Interference between outgoing and incoming signals produces an optical interferogram that measures transmission-induced phase noise, which can be removed in post-processing due to the reciprocity of the link. This method combines optical phase detection with the robustness of a pulse train, maintaining phase coherence even with pulse loss from signal fading [157]. The first optical clock comparisons over a free-space link were reported in 2021 by a NIST collaboration, comparing results from a 1.5 km free-space link and a 3.6 km fiber link [153]. Remarkably, free-space optical two-way transfer with frequency combs has since been demonstrated over distances up to 300 km [134,158], despite picowatt-level received signals [134]. Based on these results, extending this technique to ground–space–ground links via geostationary satellites appears feasible for remote optical clock comparisons [159].

3. *Transportable, High-Performance Optical Atomic Clocks*

An alternative for comparing optical clocks across continents—or in labs without access to optical fiber links—is to use transportable optical clocks. Achieving lab-level accuracy in a portable system presents significant engineering challenges, not only for the atomic package but also for developing rugged, compact optical reference cavities [160–162]. Current systems are typically the size of a large refrigerator or housed in transport vans. Despite these constraints, several transportable clocks have demonstrated systematic uncertainties below 10^{-16}, based on both lattice clocks [163–166] and trapped-ion systems [167–169], with the best reaching the low 10^{-18} level [82]. Many have been deployed for remote comparisons or used outside metrology labs in chronometric leveling experiments (Section 8.B). Only recently, however, was a transportable optical clock used in an intercontinental comparison, when a system from Japan was transported to the UK and Germany [170].

C. Status of Optical Clock Comparisons

Despite major advances in optical clock comparisons, achieving international consistency at the 5×10^{-18} level—the target set in the roadmap [24] for redefining the second—remains a challenge. Although one non-unity frequency ratio has reached this uncertainty [66] and several others have reported uncertainties below 10^{17}, independent verification is still lacking. Moreover, the scatter in frequency ratio measurements is often larger than expected from white frequency noise alone [153,171], prompting the use of methods such as Birge ratio inflation or modeling excess scatter as a time-varying "dark" uncertainty. Even in comparisons between independent realizations of clocks based on the same transition, deviations from unity often exceed those predicted by evaluated systematic uncertainties [170]. Coordinated, large-scale clock comparison campaigns, especially those involving multiple link types, are essential for identifying outliers and investigating the root causes of these discrepancies [172].

Three independently measured frequency ratios between clocks with frequencies ν_1, ν_2 and ν_3 should satisfy the relation:

$$\frac{\nu_1}{\nu_2}\frac{\nu_2}{\nu_3}\frac{\nu_3}{\nu_1} = 1. \tag{6}$$

Examination of such "loop closures" has been used to demonstrate that the frequencies of optical clocks are reproducible beyond what is achievable through comparisons against the current realization of the SI second [82]. More generally, methods have been developed to evaluate the internal self-consistency of the complete global body of clock comparison data and to derive optimized frequency ratio values from all available measurements. These methods are based either on least-squares analysis [173] or examination of closed loops in a graph theory framework [174], and to date have been applied primarily to derive the recommended frequency values used when secondary frequency standards contribute to TAI (Section 7.A). However, they will become increasingly important in assessing the consistency of optical frequency ratio measurements as progress is made toward a redefinition of the second.

7. TIMEKEEPING WITH OPTICAL CLOCKS

A. Optical Clocks in TAI

One of the primary beneficiaries of an optical redefinition of the SI second will be the global time scales TAI and UTC. Some optical clocks are already being used as secondary frequency standards to steer TAI, alongside cesium fountain primary frequency standards. In this process, agreed "recommended" values of their frequencies are used, which are derived from an analysis of the complete worldwide body of accurate clock comparison data [175]. So far, 11 optical clocks have been officially approved to contribute as secondary frequency standards. Most are strontium or ytterbium optical lattice clocks, with two ion clocks added recently. In practice, however, the number of optical clocks contributing to TAI each month remains well below the number of cesium fountain contributions. This is because most optical clocks still operate intermittently, with datasets that are often shorter than the full 30-day Circular T reporting period.

The 2021 update to the recommended frequency values [176] reduced the fractional uncertainties for strontium and ytterbium to 1.9×10^{-16}, on a par with the best cesium fountains. In principle, this would allow optical clocks to carry equal weight in TAI computation—if they achieved comparable uptime. While their robustness has improved [177], optical clocks still operate intermittently, with frequent dead time and incomplete 30-day Circular T datasets, which increase the link uncertainty through reliance on hydrogen masers [178]. As a result, very few optical contributions have so far met the target 2×10^{-16} uncertainty set in the roadmap for redefinition of the second [24]. Meeting the redefinition criterion—three contributions per month below this uncertainty for at least one year—will require sustained operation of optical clocks with high uptime across full Circular T intervals.

B. Relativistic Effects on Clocks

When comparing optical clocks, whether directly or when contributing to the TAI, the difference in the gravity potential at each clock's location must be taken into account. According to general relativity, clocks run more slowly when they are closer to Earth's center of gravity. This means that a clock at sea level ticks slightly slower than an identical clock at higher altitude. The resulting fractional frequency shift between two clocks at rest on Earth's

surface is given by

$$\frac{\Delta f_{GR}}{f} = -\frac{\Delta W}{c^2}, \tag{7}$$

where ΔW is the gravity potential difference between them and c is the speed of light in vacuum. For example, a clock at NPL in the UK, little more than 10 m above sea level, when compared to a clock at NIST in the "mile high state" of Colorado, will appear to be ticking too slowly by nearly 2 parts in 10^{13}.

TAI is defined to match Terrestrial Time, using a reference gravity potential of $W_0 = 62{,}636{,}856.0\ \mathrm{m^2 s^{-2}}$, which corresponds roughly to mean sea level [179]. When a primary or secondary frequency standard contributes to TAI, its local gravity potential must be determined relative to this reference. For cesium fountain clocks, this is relatively straightforward. But for optical clocks, which can reach fractional uncertainties below 10^{-18}, the required precision is much higher: the local gravity potential must be known to within about $0.1\ \mathrm{m^2 s^{-2}}$, which is equivalent to knowing the clock's height to within just 1 cm.

On a global scale, Earth's gravity potential is modeled using satellite data from missions like Gravity Recovery and Climate Experiment (GRACE) and Gravity Field and Ocean Circulation Explorer (GOCE) [180]. However, these models are only accurate for large-scale features, typically those spanning 200 km or more, so they lack the resolution needed to determine gravity potential precisely at the local level. To work out the gravity potential at the specific location of a clock, information from the global model must be combined with regional information from gravity measurements (to resolve variations on intermediate spatial scales of ∼50 to 200 km) and topographic data from high-resolution digital elevation models (to obtain short spatial scales from meters to 50 km) [181]. This approach has enabled the gravity potential in several European laboratories to be determined with an accuracy corresponding to better than 3×10^{-18} clock uncertainty [139]. Uncertainties below the 1×10^{-17} level, the target set in the roadmap for redefinition of the second, have also been achieved in several other laboratories [182,183].

Apart from the static part of the gravity potential, temporal variations must also be considered [184]. The largest contributions come from solid Earth tides, with ocean tides also being relevant at the 10^{-17} level. However as clock comparisons improve toward the 10^{-18} level several other time-variable potential effects can become important, such as non-tidal mass redistributions in the atmosphere due to storms or anticyclones, or variations in continental water storage on seasonal time scales. Current models and measurement of the Earth's gravity potential will therefore limit the accuracy of time realization in UTC, even after an optical redefinition of the SI second, with further improvements being necessary to reach the theoretical factor of 100 gain in accuracy.

Clock comparisons require only the difference in gravity potential between locations. However, when comparing clocks across countries, even within the same continent, resolving these differences accurately remains challenging. In contrast, for local comparisons, gravity potential differences can be determined more easily at the millimeter level in height using geometric leveling techniques.

C. Optical Time Scales and Accessibility of UTC

For optical clocks to support real-time timing services through UTC(k), they must be integrated into national time scales. As they currently operate as frequency standards rather than continuous clocks, their role will mirror that of cesium fountains—providing periodic frequency corrections to steer a continuously running microwave oscillator (hydrogen maser) [185–190]. This approach is already being used in time scales in both Japan and Korea, with UTC(NICT) being steered by a strontium optical lattice clock and UTC(KRIS) by an ytterbium optical lattice clock.

In the future, however, we can envisage fully optical time scales, where hydrogen masers are replaced by an optical alternative. Alternative systems might include low-drift cavity-stabilized lasers as in an initial demonstration of an all-optical scale time using a cryogenic silicon cavity [191]. Other promising candidates include high-uptime frequency standards with excellent short- and medium-term stability, such as thermal beam optical clocks [192], active optical clocks [96], and systems based on spectral holes in cryogenically cooled $Eu^{3+} : Y_2SiO_5$ crystals [193].

These approaches are expected to yield significant enhancements in the stability of UTC(k) time scales, to well below 1 ns as the uptime of optical clocks continues to improve. However, to make this improved performance accessible to end users, new methods for time dissemination will be required, for example, through optical fiber networks (Section 6.B.2). Important steps in this direction have already been taken in several countries, particularly in Europe. For instance, the French national Metrological Fiber Network (REFIMEVE) network in France disseminates time and frequency signals from UTC(OP) to research laboratories across the country, supporting applications in photonics, laser stabilization and control, and high-resolution atomic and molecular spectroscopy [194].

In Italy, the quantum backbone network supports both secure quantum key distribution using twin-field QKD [132], and stable time and frequency dissemination from optical clocks to radio telescopes for improved VLBI [195].

D. Options for Redefinition of the Second

Beyond the technical challenges of redefining the second, a critical question remains: what form should the new definition take? Fixing the numerical value of another fundamental constant, such as the electron mass m_e or the Rydberg constant R_∞, has been ruled out for now, as their uncertainties are still orders of magnitude larger than the current realization of the second [24]. Although c, h, e, k, and N_A have already been fixed in recent SI revisions [196,197], only two viable options for defining the second remain under consideration.

The first is to select one optical transition and to fix the numerical value of its frequency. In this case, optical frequency standards based on this particular transition will become the new primary frequency standards, and cesium fountains will become secondary frequency standards, with the cesium frequency having an uncertainty assigned in the list of recommended frequency values rather than being exactly set by the definition. This option has the advantage of simplicity, and it is easy to understand how such a definition would be applied in practice as it is a straightforward adaptation of the present definition. However with so many different optical transitions currently being worked on around the globe, it is likely to be challenging to reach consensus on the best transition to pick for the definition.

An alternative to selecting a single transition is to define the second using a fixed weighted geometric mean of several optical

transition frequencies [198], with the weights and mean forming the defining constants. This approach leverages the fact that multiple optical clocks now demonstrate comparable performance, potentially easing consensus on which transitions to include. However, the concept is less intuitive, and the form of a primary realization remains under debate. A dynamic variant, whereby means and weights are periodically updated, has also been proposed to track future improvements in clock performance. This would mark a significant departure from current SI practice, and its broader implications are still under study.

8. EMERGING APPLICATIONS OF OPTICAL CLOCKS

A. Testing Fundamental Physics

Frequency ratios between optical atomic clocks are among the most precise fractional measurements ever achieved, where fractional uncertainties below 10^{-18} correspond to energy sensitivities in the attoelectronvolt range. Because atomic transition frequencies are governed by fundamental physical laws and constants, such precision enables optical clocks to probe potential violations of general relativity, Lorentz invariance, CPT symmetry, and the constancy of fundamental constants. As a result, clock comparisons provide a complementary, high-resolution, table-top platform to high-energy experiments like the Large Hadron Collider for testing physics beyond the Standard Model.

As seen in Fig. 6, atomic clocks are intrinsically sensitive to **relativistic Doppler shifts**, including the second-order effect from time dilation. For atoms moving at velocity, v, the clock frequency experiences a fractional shift $\Delta f/f = -v^2/2c^2$. At the 10^{-18} level, even motion at the scale of centimeters per second becomes measurable. While this sensitivity requires careful control to avoid systematic errors, it also enables precision tests of Lorentz symmetry, where violations could manifest as velocity- or direction-dependent frequency shifts. Relativistic Doppler effects also play a key role in satellite-based comparisons and relativistic geodesy, where they must be disentangled from gravitational redshifts to probe for deviations from general relativity.

One of the most direct clock-based tests of general relativity is the gravitational redshift, which can be observed by comparing two clocks at different gravitational potentials. An experiment at Tokyo Skytree [199] compared two transportable strontium optical clocks, with one at the top and one at the base of the tower, and demonstrated a measurement precision of 91 parts per million. This result surpassed the fractional accuracy achieved by the 1980 Gravity Probe A rocket experiment [200] and approached that of more recent satellite-based redshift tests [201,202], even though the height difference between the clocks was only a few hundred meters. This illustrates the much higher intrinsic sensitivity of optical clocks to gravitational redshifts. Future space missions, such as ACES [142], aim to improve the uncertainty of spaceborne redshift measurements by one to two orders of magnitude. In the longer term, optical clocks deployed directly in space may offer another substantial gain in sensitivity [203], enabling more stringent tests of general relativity.

Other types of tests explore whether the fundamental constants governing atomic structure, such as the fine-structure constant, α and the proton-to-electron mass ratio $\mu = m_e/m_p$, are truly constant in time and space. Because different atomic transitions depend on these constants in different ways, comparing clocks based on different atoms enables sensitive tests for slow drifts or their coupling to a gravitational potential [52,124,204,205], as well as oscillatory and transient variations [153,206–209]. These ideas are being pursued both in long-term comparisons between optical clocks and in searches for signals linked to dark matter [153,207,208] and scalar fields.

Such variations are predicted in theories that propose new fields, like scalar fields—hypothetical energy fields that could slowly or periodically shift the values of fundamental constants. Some models also suggest that dark matter might weakly interact with normal matter ("couple" to it), producing small shifts in atomic transitions that clocks can detect. Optical clock comparisons have also been used to test Lorentz symmetry, for example, by exploiting the relative velocities of networked clocks in the geocentric frame [150], or by comparing clocks with differently oriented atomic quantization axes, which can reveal direction-dependent frequency shifts predicted by some Lorentz-violating theories [127]. It has even been proposed [210] that optical clocks with fractional instability below 10^{-20} could enable space-based gravitational wave detection, though this remains beyond current state-of-the-art performance (Fig. 6).

Emerging clock technologies discussed in Section 4.C, such as highly charged ion clocks [97] and nuclear clocks [103,104], offer significantly enhanced sensitivity to variations of fundamental constants compared to established single-ion and optical lattice clocks [211,212]. In HCIs, stronger Coulomb binding amplifies relativistic effects in the clock transition, increasing sensitivity to changes in the fine-structure constant α. Nuclear clocks go further, as their transition energies depend directly on nuclear binding forces and a broader set of constants, while benefiting from exceptional isolation due to electron cloud shielding. These features make both platforms especially promising for stringent tests of fundamental physics, including searches for ultralight scalar fields, time-varying constants, and violations of Lorentz and CPT symmetry.

B. Optical Clocks as Gravity Sensors

The importance of accounting for gravitational effects when comparing optical clocks, or when using them for international timekeeping, has already been discussed in Section 7.B. However, the connection between clocks and gravity also works in the opposite direction: optical clocks with well-characterized uncertainty budgets at the level of 1×10^{-18} can serve as sensitive probes of the gravity potential [213].

Unlike gravimeters, which measure the local acceleration due to gravity (the derivative of the potential) [214], optical clocks respond directly to the gravity potential itself. Clock-based gravity measurements have potential applications in establishing a unified international height reference system—one based on gravity potential rather than sea level. This would help connect tide gauges that currently define national height systems, many of which disagree by several decimetres due to differences in local sea-level and historical measurement practices, even within a single continent [213]. Optical clocks could also enable high-resolution mapping of the gravity potential in mountainous regions with complex terrain [215].

A first proof-of-principle chronometric leveling experiment used a transportable strontium optical lattice clock, linked via optical fiber, to measure the gravity potential difference between

two locations: one situated in the mountains and another approximately 90 km away and 1000 m lower in altitude [216]. In this experiment, both local and remote clock comparisons were performed to eliminate susceptibility to any potential clock errors. However, the performance of the transportable clock in this experiment limited the accuracy of the clock comparisons that could be performed, falling short of what could be derived by traditional geodetic methods. Transportable optical clocks with better accuracy, able to resolve height differences at the cm-level, were demonstrated at Tokyo Skytree broadcasting tower (Section 8.A).

Recently, a lab-based optical lattice clock was employed to resolve gravitational frequency shifts at the millimeter scale within a single atomic sample [217]. While this experiment is remarkable in resolution, it only captures highly localized changes in the gravity potential, not the broader variations across Earth's surface that geodetic applications require.

With continued improvements in the environmental robustness of transportable optical clocks and the use of synchronous interrogation techniques that suppress certain sources of instability [77], their application to establishing consistent international height reference systems appears increasingly feasible. Further gains in clock stability could also enable detection of time-varying changes in Earth's gravity potential, such as those caused by solid Earth tides [213].

C. Compact and Portable Optical Clocks for Holdover

Although gravity sensing demands optical clocks with state-of-the-art stability and accuracy, other applications may prioritize cost, size, weight, and power consumption (C-SWaP) over performance. For example, free access to GNSS timing signals has revolutionized industries, transformed daily life, and generated enormous economic value, largely due to their global reach and ease of use. Within this success, however, lie some dangers: modern infrastructure has become highly dependent on satellite signals that are weak and susceptible to disruption.

Compact and portable atomic clocks can help fill this gap. They are especially useful in environments where GNSS cannot reach, such as underground, underwater, or inside buildings. Another critical application is holdover timing, which maintains accurate time during GNSS outages, whether caused by natural events like solar storms or intentional interference from malicious actors.

Compact and portable microwave atomic clocks have been available commercially for decades, whereas portable optical atomic clocks are at a relatively early stage of development. However, some systems are already showing performance on a par with the best microwave atomic clocks [218,219], and have been tested in a maritime environment [220,221], demonstrating short-term fractional frequency stability better than $10^{-13}/\sqrt{\tau}$, comparable to a hydrogen maser but in packages significantly smaller and lighter. These systems use robust thermal-vapor-cell technology rather than the laser-cooled atoms employed in state-of-the-art optical atomic clocks, and are based on reference transitions in molecular iodine [220], rubidium, or ytterbium [221]. Successful operation of an iodine frequency reference has also been demonstrated on a sounding rocket mission [222], a first step toward future space deployment. Finally, recent efforts are starting to translate the success of the microwave chip-scale atomic clock (CSAC) into the optical domain [223].

Optical clocks offer key advantages over traditional microwave systems. Shorter wavelengths allow more compact components, and higher-frequency transitions lead to sharper resonances and higher quality factors (Q), improving operational stability. For portable systems, the required small length scale sets a limited interaction time which makes the higher frequency of the transition essential to achieving a high transition Q. Additionally, because optical transitions operate at much higher frequencies, environmental shifts result in smaller fractional errors, enabling clocks to be more robust against external perturbations.

However, the optical approach presents significant challenges for compact and high-performance systems. Chief among them is increased system complexity, particularly the need to convert the optical clock signal to frequencies usable by electronic systems. This requires a compact, robust frequency comb, making the development of integrated microcombs [224] and high-performance monolithic mode-locked laser for OFCs [225] a critical step forward. In addition to compact comb sources, compact and stable optical references are also required for clock interrogation. Recent developments include air-gap, centimeter-scale reference cavities capable of thermal-noise-limited instabilities in the low $\times 10^{-14}$-level without the need for ion pumps [226]. Additionally, optical clocks have been interrogated using a microresonator-based system employing stimulated Brillouin scattering [227] and a chip-integrated, waveguide spiral optical reference [228]. When used to probe the $^{88}Sr^{+}$ transition, both systems demonstrated fractional instabilities on the order of $4 \times 10^{-14}\tau^{-1/2}$.

Finally, the supply chains for critical components are underdeveloped, resulting in higher costs. Optical components must be matched to the specific wavelengths of clock transitions, which typically lie outside standard telecommunications bands making it difficult to take advantage of the cost and reliability benefits of the optical communications industry. However, parallel development needs for other photonic applications like quantum computing and biosciences are likely to improve the availability and cost of the components needed for optical clocks, leading to more affordable and accessible systems in the future.

9. TIME AND METROLOGY: OUTLOOK

Optical atomic clocks have advanced rapidly since their inception and now offer groundbreaking precision at a table-top scale. The best systems have achieved fractional uncertainties below 10^{-18} and fractional instabilities approaching $5 \times 10^{-17}\tau^{-1/2}$. While the quantum limits to statistical precision are well understood, ongoing work in entanglement of ions within the same trap [229], quantum networking of independent clocks [230] and spin squeezing [231] aims to improve stability beyond the standard quantum projection noise limit. At the same time, accuracy at the 10^{-19} level and beyond will push the ultimate limits of systematic control and motivate advances in clock design, modeling, and environmental isolation.

The rapid gains in performance observed over the past four decades have enabled optical atomic clocks to support both practical applications, such as international timekeeping, and fundamental tests of physics. A decade ago, none contributed to the steering of international atomic time; today, 11 have been approved—nearly matching the number of cesium fountain standards—and a roadmap for redefining the second is underway. However, key challenges remain: deciding between a single-species or ensemble-based redefinition, demonstrating consistency at the 5×10^{-18} level through high-accuracy comparisons, and

improving clock robustness to match the reliability of cesium fountains.

Optical atomic clocks are already pushing the limits of our physical understanding by testing whether the fundamental forces vary over time, placing constraints on possible interactions with dark matter, and enabling new approaches in relativistic geodesy. Expanding access to optical clocks through advanced time and frequency dissemination, compact portable systems, and planned space-based implementations [232,233] is poised to enable a broad range of impactful new applications.

The continued advancement of optical clocks presents a compelling opportunity for the laser and photonics community to drive progress at the frontier of precision measurement. Meeting the demands of next-generation systems will require innovation in laser stabilization, integrated optics, and low-noise detection. As clocks move beyond the laboratory and into real-world platforms and networks, the technologies developed to support them will shape not only the future of timekeeping, but also the broader scientific and technological systems that support emerging applications across disciplines.

Funding. Department for Science, Innovation and Technology; Australian Research Council (CE230100006).

Acknowledgment. The authors would like to acknowledge Dave Hume, Nick Nardelli, Ben Stein, Giulio Tagliaferro, Mike Lombardi, Ladan Arissian, Geoffrey Barwood, and Rachel Godun for careful reading of the paper. Tara M. Fortier acknowledges funding and support from the National Institute of Science and Technology, Physical Measurement Laboratory. Andre Luiten acknowledges the University of Adelaide, Institute for Photonics and Advanced Sensing, Defence Science and Technology Group, and the Australian Government through the Australian Research Council Centre of Excellence in Optical Microcombs for Breakthrough Science (project number CE230100006) for ongoing support of his research. Helen S. Margolis acknowledges funding from the UK government Department for Science, Innovation, and Technology (DSIT) through the National Measurement System Programme.

Disclosures. Andre Luiten is co-founder, part owner, and CEO of QuantX Labs Pty Ltd. QuantX holds commercial intellectual property rights to portable optical clock technology that was developed at the University of Adelaide.

Data availability. This review paper does not present new experimental or computational data. All results and numerical values discussed here are taken from previously published sources, which are cited throughout the text.

REFERENCES

1. J. Kovalevsky, "Astronomical time," Metrologia **1**, 169 (1965).
2. D. D. McCarthy, "Evolution of timescales from astronomy to physical metrology," Metrologia **48**, S132 (2011).
3. P. Tavella and J. X. Mitrovica, "Melting ice solves leap-second problem—for now," Nature **628**, 273–274 (2024).
4. J. Levine, P. Tavella, and M. Milton, "Towards a consensus on a continuous coordinated universal time," Metrologia **60**, 014001 (2023).
5. L. Essen and J. Parry, "An atomic standard of frequency and time interval: a caesium resonator," Nature **176**, 280–282 (1955).
6. C. H. Townes, "Production of coherent radiation by atoms and molecules," Science **149**, 831–841 (1965).
7. N. G. Basov, "Semiconductor lasers," Science **149**, 821–827 (1965).
8. A. M. Prokhorov, "Quantum electronics," Science **149**, 828–830 (1965).
9. A. Kastler, "Optical methods for studying hertzian resonances," Science **158**, 214–221 (1967).
10. N. Bloembergen, "Nonlinear optics and spectroscopy," Rev. Mod. Phys. **54**, 685–695 (1982).
11. A. L. Schawlow, "Spectroscopy in a new light," Rev. Mod. Phys. **54**, 697–707 (1982).
12. N. F. Ramsey, "Experiments with separated oscillatory fields and hydrogen masers," Rev. Mod. Phys. **62**, 541–552 (1990).
13. H. Dehmelt, "Experiments with an isolated subatomic particle at rest," Rev. Mod. Phys. **62**, 525–530 (1990).
14. W. Paul, "Electromagnetic traps for charged and neutral particles," Rev. Mod. Phys. **62**, 531–540 (1990).
15. S. Chu, "Nobel lecture: the manipulation of neutral particles," Rev. Mod. Phys. **70**, 685–706 (1998).
16. C. N. Cohen-Tannoudji, "Nobel lecture: manipulating atoms with photons," Rev. Mod. Phys. **70**, 707–719 (1998).
17. W. D. Phillips, "Nobel lecture: laser cooling and trapping of neutral atoms," Rev. Mod. Phys. **70**, 721–741 (1998).
18. J. L. Hall, "Nobel lecture: defining and measuring optical frequencies," Rev. Mod. Phys. **78**, 1279–1295 (2006).
19. T. W. Hänsch, "Nobel lecture: passion for precision," Rev. Mod. Phys. **78**, 1297–1309 (2006).
20. S. Haroche, "Nobel lecture: controlling photons in a box and exploring the quantum to classical boundary," Rev. Mod. Phys. **85**, 1083–1102 (2013).
21. D. J. Wineland, "Nobel lecture: superposition, entanglement, and raising Schrödinger's cat," Rev. Mod. Phys. **85**, 1103–1114 (2013).
22. A. Aeppli, K. Kim, W. Warfield, *et al.*, "Clock with 8×10^{-19} systematic uncertainty," Phys. Rev. Lett. **133**, 023401 (2024).
23. M. C. Marshall, D. A. R. Castillo, W. J. Arthur-Dworschack, *et al.*, "High-stability single-ion clock with 8×10^{-19} systematic uncertainty," Phys. Rev. Lett. **135**, 033201 (2025).
24. N. Dimarcq, M. Gertsvolf, G. Mileti, *et al.*, "Roadmap towards the redefinition of the second," Metrologia **61**, 012001 (2024).
25. N. Poli, C. W. Oates, P. Gill, *et al.*, "Optical atomic clocks," La Rivista Nuovo Cimento **36**, 555–624 (2013).
26. A. D. Ludlow, M. M. Boyd, J. Ye, *et al.*, "Optical atomic clocks," Rev. Mod. Phys. **87**, 637–701 (2015).
27. W. J. Riley, *Handbook of Frequency Stability Analysis* (US Department of Commerce, National Institute of Standards and Technology, 2008).
28. IEEE, "IEEE 1139-2022, IEEE standard definitions of physical quantities for fundamental frequency and time metrology–random instabilities," https://standards.ieee.org/ieee/1139/7585/ (2022).
29. D. Wineland and H. Dehmelt, "Proposed $10^{14}\delta\nu/\nu$ laser fluorescence spectroscopy on Tl^+ mono-ion oscillator III," Bull. Am. Phys. Soc. **20**, 637 (1975).
30. T. W. Hänsch and A. L. Schawlow, "Cooling of gases by laser radiation," Opt. Commun. **13**, 68–69 (1975).
31. D. J. Wineland, R. E. Drullinger, and F. L. Walls, "Radiation-pressure cooling of bound resonant absorbers," Phys. Rev. Lett. **40**, 1639 (1978).
32. W. Neuhauser, M. Hohenstatt, P. Toschek, *et al.*, "Optical-sideband cooling of visible atom cloud confined in parabolic well," Phys. Rev. Lett. **41**, 233 (1978).
33. W. D. Phillips and H. Metcalf, "Laser deceleration of an atomic beam," Phys. Rev. Lett. **48**, 596–599 (1982).
34. R. Dicke, "The effect of collisions upon the Doppler width of spectral lines," Phys. Rev. **89**, 472 (1953).
35. N. F. Ramsey, "A molecular beam resonance method with separated oscillating fields," Phys. Rev. **78**, 695 (1950).
36. V. Giovannetti, S. Lloyd, and L. Maccone, "Quantum-enhanced measurements: beating the standard quantum limit," Science **306**, 1330–1336 (2004).
37. S. M. Brewer, J.-S. Chen, A. M. Hankin, *et al.*, "$^{27}Al^+$ quantum-logic clock with a systematic uncertainty below 10^{-18}," Phys. Rev. Lett. **123**, 033201 (2019).
38. T. L. Nicholson, S. Campbell, R. Hutson, *et al.*, "Systematic evaluation of an atomic clock at 2×10^{-18} total uncertainty," Nat. Commun. **6**, 6896 (2015).
39. E. Oelker, R. B. Hutson, C. J. Kennedy, *et al.*, "Demonstration of stability at 1 s for two independent optical clocks," Nat. Photonics **13**, 714–719 (2019).
40. A. Quessada, R. P. Kovacich, I. Courtillot, *et al.*, "The Dick effect for an optical frequency standard," J. Opt. B Quantum Semiclass. Opt. **5**, S150 (2003).
41. G. J. Dick, "Local oscillator induced instabilities in trapped ion frequency standards," in *Proceedings of the 19th Annual Precise Time and Time Interval Systems and Applications Meeting* (1989), pp. 133–147.

42. H. Dehmelt, "Proposed $10^{14}\delta\nu/\nu$ laser fluorescence spectroscopy on Tl^+ mono-ion oscillator," Bull. Am. Phys. Soc. **18**, 1521 (1973).
43. H. Dehmelt, "Proposed $10^{14}\delta\nu/\nu$ laser fluorescence spectroscopy on Tl^+ mono-ion oscillator," Bull. Am. Phys. Soc. **20**, 60 (1975).
44. H. G. Dehmelt, "Mono-ion oscillator as potential ultimate laser frequency standard," IEEE Trans. Instrum. Meas. **IM-31**, 83–87 (1982).
45. N. Herschbach, K. Pyka, J. Keller, *et al.*, "Linear Paul trap design for an optical clock with Coulomb crystals," Appl. Phys. B **107**, 891–906 (2012).
46. K. Matsubara, K. Hayasaka, Y. Li, *et al.*, "Frequency measurement of the optical clock transition of $^{40}Ca^+$ ions with an uncertainty of 10^{-14} level," Appl. Phys. Express **1**, 067011 (2008).
47. H. Margolis, G. Huang, G. Barwood, *et al.*, "Absolute frequency measurement of the 674-nm clock transition using a femtosecond optical frequency comb," Phys. Rev. A **67**, 032501 (2003).
48. A. A. Madej, J. E. Bernard, P. Dubé, *et al.*, "Absolute frequency of the $^{88}Sr^+5s^2S_{1/2}$–$4d^2D_{5/2}$ reference transition at 445 THz and evaluation of systematic shifts," Phys. Rev. A **70**, 012507 (2004).
49. C. Tamm, N. Huntemann, B. Lipphardt, *et al.*, "Cs-based optical frequency measurement using cross-linked optical and microwave oscillators," Phys. Rev. A **89**, 023820 (2014).
50. S. A. Diddams, T. Udem, J. Bergquist, *et al.*, "An optical clock based on a single trapped $^{199}Hg^+$ ion," Science **293**, 825–828 (2001).
51. K. J. Arnold, R. Kaewuam, S. R. Chanu, *et al.*, "Precision measurements of the $^{138}Ba^+6s^2S_{1/2}$–$5d^2D_{5/2}$ clock transition," Phys. Rev. Lett. **124**, 193001 (2020).
52. R. M. Godun, P. B. R. Nisbet-Jones, J. M. Jones, *et al.*, "Frequency ratio of two optical clock transitions in and constraints on the time variation of fundamental constants," Phys. Rev. Lett. **113**, 210801 (2014).
53. J. Von Zanthier, T. Becker, M. Eichenseer, *et al.*, "Absolute frequency measurement of the In^+ clock transition with a mode-locked laser," Opt. Lett. **25**, 1729–1731 (2000).
54. T. Rosenband, P. O. Schmidt, D. B. Hume, *et al.*, "Observation of the $^1S_0$–$^3P_0$ clock transition in $^{27}Al^+$," Phys. Rev. Lett. **98**, 220801 (2007).
55. K. J. Arnold, R. Kaewuam, A. Roy, *et al.*, "Observation of the $^1S_0$ to $^3D_1$ clock transition in $^{175}Lu^+$," Phys. Rev. A **94**, 052512 (2016).
56. D. J. Berkeland, J. D. Miller, J. C. Bergquist, *et al.*, "Minimization of ion micromotion in a Paul trap," J. Appl. Phys. **83**, 5025–5033 (1998).
57. S. Stenholm, "The semiclassical theory of laser cooling," Rev. Mod. Phys. **58**, 699 (1986).
58. D. Wineland, W. M. Itano, J. Bergquist, *et al.*, "Laser-cooling limits and single-ion spectroscopy," Phys. Rev. A **36**, 2220 (1987).
59. W. M. Itano, "External-field shifts of the $^{199}Hg^+$ optical frequency standard," J. Res. Natl. Inst. Stand. Technol. **105**, 829–837 (2000).
60. P. Dubé, A. A. Madej, J. E. Bernard, *et al.*, "Electric quadrupole shift cancellation in single-ion optical frequency standards," Phys. Rev. Lett. **95**, 033001 (2005).
61. P. O. Schmidt, T. Rosenband, C. Langer, *et al.*, "Spectroscopy using quantum logic," Science **309**, 749–752 (2005).
62. N. Ohtsubo, Y. Li, K. Matsubara, *et al.*, "Frequency measurement of the clock transition of an indium ion sympathetically-cooled in a linear trap," Opt. Express **25**, 11725–11735 (2017).
63. Z. Y. Ma, K. Deng, Z. Y. Wang, *et al.*, "Quantum-logic-based $^{25}Mg^+$–$^{27}Al^+$ optical frequency standard for the redefinition of the SI second," Phys. Rev. Appl. **21**, 044017 (2024).
64. A. Tofful, C. F. A. Baynham, E. A. Curtis, *et al.*, "$^{171}Yb^+$ optical clock with 2.2×10^{-18} systematic uncertainty and absolute frequency measurements," Metrologia **61**, 045001 (2024).
65. N. Huntemann, C. Sanner, B. Lipphardt, *et al.*, "Single-ion atomic clock with 3×10^{-18} systematic uncertainty," Phys. Rev. Lett. **116**, 063001 (2016).
66. H. N. Hausser, J. Keller, T. Nordmann, *et al.*, "$^{115}In^+$–$^{172}Yb^+$ Coulomb crystal clock with 2.5×10^{-18} systematic uncertainty," Phys. Rev. Lett. **134**, 023201 (2025).
67. Y. Huang, B. Zhang, M. Zeng, *et al.*, "Liquid-nitrogen-cooled Ca^+ optical clock with systematic uncertainty of 3×10^{-18}," Phys. Rev. Appl. **17**, 034041 (2022).
68. J. Keller, T. Burgermeister, D. Kalincev, *et al.*, "Controlling systematic frequency uncertainties at the 10^{-19} level in linear Coulomb crystals," Phys. Rev. A **99**, 013405 (2019).
69. K. Arnold, E. Hajiyev, E. Paez, *et al.*, "Prospects for atomic clocks based on large ion crystals," Phys. Rev. A **92**, 032108 (2015).
70. D. R. Leibrandt, S. G. Porsev, C. Cheung, *et al.*, "Prospects of a thousand-ion Coulomb-crystal clock with sub- inaccuracy," Nat. Commun. **15**, 5663 (2024).
71. H. Katori, "Optical lattice clocks and quantum metrology," Nat. Photonics **5**, 203–210 (2011).
72. H. Katori, "Spectroscopy of strontium atoms in the Lamb-Dicke confinement," in *Frequency Standards and Metrology* (World Scientific, 2002), pp. 323–330.
73. X. Baillard, M. Fouché, R. L. Targat, *et al.*, "Accuracy evaluation of an optical lattice clock with bosonic atoms," Opt. Lett. **32**, 1812–1814 (2007).
74. Z. W. Barber, C. W. Hoyt, C. W. Oates, *et al.*, "Direct excitation of the forbidden clock transition in neutral atoms confined to an optical lattice," Phys. Rev. Lett. **96**, 083002 (2006).
75. M. Takamoto, F.-L. Hong, R. Higashi, *et al.*, "An optical lattice clock," Nature **435**, 321–324 (2005).
76. W. McGrew, X. Zhang, R. Fasano, *et al.*, "Atomic clock performance enabling geodesy below the centimetre level," Nature **564**, 87–90 (2018).
77. T. Takano, M. Takamoto, I. Ushijima, *et al.*, "Geopotential measurements with synchronously linked optical lattice clocks," Nat. Photonics **10**, 662–666 (2016).
78. J. Li, X.-Y. Cui, Z.-P. Jia, *et al.*, "A strontium lattice clock with both stability and uncertainty below 5×10^{-18}," Metrologia **61**, 015006 (2024).
79. I. Ushijima, M. Takamoto, M. Das, *et al.*, "Cryogenic optical lattice clocks," Nat. Photonics **9**, 185–189 (2015).
80. Y. S. Hassan, K. Beloy, J. L. Siegel, *et al.*, "Cryogenic optical lattice clock with 1.7×10^{-20} blackbody radiation stark uncertainty," arXiv (2025).
81. R. Tyumenev, M. Favier, S. Bilicki, *et al.*, "Comparing a mercury optical lattice clock with microwave and optical frequency standards," New J. Phys. **18**, 113002 (2016).
82. N. Ohmae, F. Bregolin, N. Nemitz, *et al.*, "Direct measurement of the frequency ratio for Hg and Yb optical lattice clocks and closure of the Hg/Yb/Sr loop," Opt Express **28**, 15112–15121 (2020).
83. A. Kulosa, D. Fim, K. Zipfel, *et al.*, "Towards a Mg lattice clock: observation of the $^1S_0$–$^3P_0$ transition and determination of the magic wavelength," Phys. Rev. Lett. **115**, 240801 (2015).
84. A. Golovizin, E. Fedorova, D. Tregubov, *et al.*, "Inner-shell clock transition in atomic thulium with a small blackbody radiation shift," Nat. Commun. **10**, 1724 (2019).
85. A. Yamaguchi, M. Safronova, K. Gibble, *et al.*, "Narrow-line cooling and determination of the magic wavelength of Cd," Phys. Rev. Lett. **123**, 113201 (2019).
86. A. D. Ludlow, N. D. Lemke, J. A. Sherman, *et al.*, "Cold-collision-shift cancellation and inelastic scattering in a Yb optical lattice clock," Phys. Rev. A **84**, 052724 (2011).
87. S. L. Campbell, R. Hutson, G. Marti, *et al.*, "A Fermi-degenerate three-dimensional optical lattice clock," Science **358**, 90–94 (2017).
88. T. Bothwell, B. D. Hunt, J. L. Siegel, *et al.*, "Lattice light shift evaluations in a dual-ensemble Yb optical lattice clock," Phys. Rev. Lett. **134**, 033201 (2025).
89. C.-C. Chen, R. Takeuchi, S. Okaba, *et al.*, "Narrow-line-mediated Sisyphus cooling in the p 2 3 metastable state of strontium," Phys. Rev. Res **7**, L022076 (2025).
90. C.-C. Chen, J. L. Siegel, B. D. Hunt, *et al.*, "Clock-line-mediated Sisyphus cooling," Phys. Rev. Lett. **133**, 053401 (2024).
91. M. Schioppo, R. C. Brown, W. F. McGrew, *et al.*, "Ultrastable optical clock with two cold-atom ensembles," Nat. Photonics **11**, 48–52 (2017).
92. H. Katori, "Longitudinal Ramsey spectroscopy of atoms for continuous operation of optical clocks," Appl. Phys Express **14**, 072006 (2021).
93. S. Okaba, R. Takeuchi, S. Tsuji, *et al.*, "Continuous generation of an ultracold atomic beam using crossed moving optical lattices," Phys. Rev. Appl. **21**, 034006 (2024).
94. A. W. Young, W. J. Eckner, W. R. Milner, *et al.*, "Half-minute-scale atomic coherence and high relative stability in a tweezer clock," Nature **588**, 408–413 (2020).
95. A. M. Kaufman and K.-K. Ni, "Quantum science with optical tweezer arrays of ultracold atoms and molecules," Nat. Phys. **17**, 1324–1333 (2021).
96. J. Zhang, T. Shi, J. Miao, *et al.*, "Active optical clock: seventeen years of progress and next steps," J. Phys. Conf. Ser. **2889**, 012035 (2024).

97. S. A. King, L. J. Spieß, P. Micke, *et al.*, "An optical atomic clock based on a highly charged ion," Nature **611**, 43–47 (2022).
98. J. L. Miller, "Slow-motion spectroscopy paves the way for a nuclear clock," Phys. Today **77**, 12–14 (2024).
99. E. Gibney, "'Nuclear clock' breakthrough paves the way for super-precise timekeeping," Nature **633**, 262–263 (2024).
100. P. Thirolf, "Shedding light on the thorium-229 nuclear clock isomer," Physics **17**, 71 (2024).
101. E. Peik and C. Tamm, "Nuclear laser spectroscopy of the 3.5 eV transition in Th-229," Europhys. Lett. **61**, 181 (2003).
102. E. Peik, T. Schumm, M. S. Safronova, *et al.*, "Nuclear clocks for testing fundamental physics," Quantum Sci. Technol. **6**, 034002 (2021).
103. J. Tiedau, M. V. Okhapkin, K. Zhang, *et al.*, "Laser excitation of the Th-229 nucleus," Phys. Rev. Lett. **132**, 182501 (2024).
104. C. Zhang, T. Ooi, J. S. Higgins, *et al.*, "Frequency ratio of the ^{229m}Th nuclear isomeric transition and the ^{87}Sr atomic clock," Nature **633**, 63–70 (2024).
105. C. Gohle, T. Udem, M. Herrmann, *et al.*, "A frequency comb in the extreme ultraviolet," Nature **436**, 234–237 (2005).
106. R. W. Drever, J. L. Hall, F. V. Kowalski, *et al.*, "Laser phase and frequency stabilization using an optical resonator," Appl. Phys. B **31**, 97–105 (1983).
107. B. Young, F. Cruz, W. Itano, *et al.*, "Visible lasers with subhertz linewidths," Phys. Rev. Lett. **82**, 3799 (1999).
108. K. Numata, A. Kemery, and J. Camp, "Thermal-noise limit in the frequency stabilization of lasers with rigid cavities," Phys. Rev. Lett. **93**, 250602 (2004).
109. T. Kessler, T. Legero, and U. Sterr, "Thermal noise in optical cavities revisited," J. Opt. Soc. Am. B **29**, 178–184 (2012).
110. G. D. Cole, W. Zhang, M. J. Martin, *et al.*, "Tenfold reduction of Brownian noise in high-reflectivity optical coatings," Nat. Photonics **7**, 644–650 (2013).
111. S. Häfner, S. Falke, C. Grebing, *et al.*, "8×10^{-17} fractional laser frequency instability with a long room-temperature cavity," Opt. Lett. **40**, 2112–2115 (2015).
112. M. Schioppo, J. Kronjäger, A. Silva, *et al.*, "Comparing ultrastable lasers at fractional frequency instability through a 2220 km optical fibre network," Nat. Commun. **13**, 212 (2022).
113. D. G. Matei, T. Legero, S. Häfner, *et al.*, "lasers with sub-10 mHz linewidth," Phys. Rev. Lett. **118**, 263202 (2017).
114. J. Valencia, G. Iskander, N. V. Nardelli, *et al.*, "Cryogenic sapphire optical reference cavity with crystalline coatings at 1×10^{-16} fractional frequency instability," Rev. Sci. Instrum. **95**, 103002 (2024).
115. H. Schnatz, B. Lipphardt, J. Helmcke, *et al.*, "First phase-coherent frequency measurement of visible radiation," Phys. Rev. Lett. **76**, 18 (1996).
116. D. J. Jones, S. A. Diddams, J. K. Ranka, *et al.*, "Carrier-envelope phase control of femtosecond mode-locked lasers and direct optical frequency synthesis," Science **288**, 635–639 (2000).
117. J. K. Ranka, R. S. Windeler, and A. J. Stentz, "Visible continuum generation in air–silica microstructure optical fibers with anomalous dispersion at 800 nm," Opt. Lett. **25**, 25–27 (2000).
118. J. Stenger, H. Schnatz, C. Tamm, *et al.*, "Ultraprecise measurement of optical frequency ratios," Phys. Rev. Lett. **88**, 073601 (2002).
119. H. Leopardi, J. Davila-Rodriguez, F. Quinlan, *et al.*, "Single-branch Er:fiber frequency comb for precision optical metrology with 10^{-18} fractional instability," Optica **4**, 879–885 (2017).
120. T. Fortier and E. Baumann, "20 years of developments in optical frequency comb technology and applications," Commun. Phys. **2**, 153 (2019).
121. T. M. Fortier, M. S. Kirchner, F. Quinlan, *et al.*, "Generation of ultrastable microwaves via optical frequency division," Nat. Photonics **5**, 425–429 (2011).
122. X. Xie, R. Bouchand, D. Nicolodi, *et al.*, "Photonic microwave signals with zeptosecond-level absolute timing noise," Nat. Photonics **11**, 44–47 (2017).
123. T. Nakamura, J. Davila-Rodriguez, H. Leopardi, *et al.*, "Coherent optical clock down-conversion for microwave frequencies with 10^{-18} instability," Science **368**, 889–892 (2020).
124. R. Schwarz, S. Dörscher, A. Al-Masoudi, *et al.*, "Long term measurement of the ^{87}Sr clock frequency at the limit of primary Cs clocks," Phys. Rev. Res. **2**, 033242 (2020).
125. R. Lange, N. Huntemann, J. M. Rahm, *et al.*, "Improved limits for violations of local position invariance from atomic clock comparisons," Phys. Rev. Lett. **126**, 011102 (2021).
126. Z. Zhiqiang, K. J. Arnold, R. Kaewuam, *et al.*, "^{176}Lu$^+$ clock comparison at the 10^{-18} level via correlation spectroscopy," Sci. Adv. **9**, eadg1971 (2023).
127. C. Sanner, N. Huntemann, R. Lange, *et al.*, "Optical clock comparison for Lorentz symmetry testing," Nature **567**, 204–208 (2019).
128. G. Petit, "Sub-10–16 accuracy GNSS frequency transfer with IPPP," GPS Solut. **25**, 22 (2021).
129. IST-SIM Time, "SIM time and frequency metrology working group," [accessed 19 January 2025], https://tf.nist.gov/sim/.
130. B. Patla, "Private communication," Conversation with the author (Private communication, 2025).
131. T. Hobiger, C. Rieck, R. Haas, *et al.*, "Combining GPS and VLBI for inter-continental frequency transfer," Metrologia **52**, 251 (2015).
132. C. Clivati, A. Meda, S. Donadello, *et al.*, "Coherent phase transfer for real-world twin-field quantum key distribution," Nat. Commun. **13**, 157 (2022).
133. C. Clivati, A. Tampellini, A. Mura, *et al.*, "Optical frequency transfer over submarine fiber links," Optica **5**, 893–901 (2018).
134. E. D. Caldwell, J.-D. Deschenes, J. Ellis, *et al.*, "Quantum-limited optical time transfer for future geosynchronous links," Nature **618**, 721–726 (2023).
135. J. Leute, N. Huntemann, B. Lipphardt, *et al.*, "Frequency comparison of ^{171}Yb$^+$ ion optical clocks at PTB and NPL via GPS PPP," IEEE Trans. Ultrason. Ferroelectr. Freq. Control **63**, 981–985 (2016).
136. J. Ray and K. Senior, "Geodetic techniques for time and frequency comparisons using GPS phase and code measurements," Metrologia **42**, 215–232 (2005).
137. G. Petit, A. Kanj, S. Loyer, *et al.*, "frequency transfer by GPS PPP with integer ambiguity resolution," Metrologia **52**, 301–309 (2015).
138. M. Fujieda, S.-H. Yang, T. Gotoh, *et al.*, "Advanced satellite-based frequency transfer at the 10^{-16} level," IEEE Trans. Ultrason. Ferroelectr. Freq. Control **65**, 973–978 (2016).
139. F. Riedel, A. Al-Masoudi, E. Benkler, *et al.*, "Direct comparisons of European primary and secondary frequency standards via satellite techniques," Metrologia **57**, 045005 (2020).
140. M. Pizzocaro, M. Sekido, K. Takefuji, *et al.*, "Intercontinental comparison of optical atomic clocks through very long baseline interferometry," Nat. Phys. **17**, 223–227 (2021).
141. P. Laurent, D. Massonnet, L. Cacciapuoti, *et al.*, "The ACES/PHARAO space mission," C.R. Phys. **16**, 540–552 (2015).
142. L. Cacciapuoti, A. Busso, R. Jansen, *et al.*, "Atomic clock ensemble in space," J. Phys. Conf. Ser. **2889**, 012005 (2024).
143. E. D. Caldwell, T. M. Triano, and L. C. Sinclair, "High-precision optical time and frequency transfer," Adv. Opt. Photonics **17**, 375–440 (2025).
144. L.-S. Ma, P. Jungner, J. Ye, *et al.*, "Delivering the same optical frequency at two places: accurate cancellation of phase noise introduced by an optical fiber or other time-varying path," Opt. Lett. **19**, 1777–1779 (1994).
145. J. Ye, J.-L. Peng, R. J. Jones, *et al.*, "Delivery of high-stability optical and microwave frequency standards over an optical fiber network," J. Opt. Soc. Am. B **20**, 1459–1467 (2003).
146. N. R. Newbury, P. A. Williams, and W. C. Swann, "Coherent transfer of an optical carrier over 251 km," Opt. Lett. **32**, 3056–3058 (2007).
147. G. Grosche, O. Terra, K. Predehl, *et al.*, "Optical frequency transfer via 146 km fiber link with relative accuracy," Opt. Lett. **34**, 2270–2272 (2009).
148. M. Musha, F.-L. Hong, K. Nakagawa, *et al.*, "Coherent optical frequency transfer over 50-km physical distance using a 120-km-long installed telecom fiber network," Opt. Express **16**, 16459–16466 (2008).
149. C. Lisdat, G. Grosche, N. Quintin, *et al.*, "A clock network for geodesy and fundamental science," Nat. Commun. **7**, 12443 (2016).
150. P. Delva, J. Lodewyck, S. Bilicki, *et al.*, "Test of special relativity using a fiber network of optical clocks," Phys. Rev. Lett. **118**, 221102 (2017).
151. C. Clivati, M. Pizzocaro, E. Bertacco, *et al.*, "Coherent optical-fiber link across Italy and France," Phys. Rev. Appl. **18**, 054009 (2022).
152. K. Predehl, G. Grosche, S. Raupach, *et al.*, "A 920-kilometer optical fiber link for frequency metrology at the 19th decimal place," Science **336**, 441–444 (2012).
153. Boulder Atomic Clock Optical Network (BACON) Collaboration, "Frequency ratio measurements at 18-digit accuracy using an optical clock network," Nature **591**, 564–569 (2021).

154. D. Gozzard, S. Schediwy, B. Stone, *et al.*, "Stabilized free-space optical frequency transfer," Phys. Rev. Appl. **10**, 024046 (2018).
155. B. P. Dix-Matthews, S. W. Schediwy, D. R. Gozzard, *et al.*, "Point-to-point stabilized optical frequency transfer with active optics," Nat. Commun. **12**, 515 (2021).
156. E. Samain, P. Exertier, C. Courde, *et al.*, "Time transfer by laser link: a complete analysis of the uncertainty budget," Metrologia **52**, 423–432 (2015).
157. F. R. Giorgetta, W. C. Swann, L. C. Sinclair, *et al.*, "Optical two-way time and frequency transfer over free space," Nat. Photonics **7**, 434–438 (2013).
158. Q. Shen, J.-Y. Guan, J.-G. Ren, *et al.*, "Free-space dissemination of time and frequency with 10^{-19} instability over 113 km," Nature **610**, 661–666 (2022).
159. E. D. Caldwell, L. C. Sinclair, J.-D. Deschenes, *et al.*, "Application of quantum-limited optical time transfer to space-based optical clock comparisons and coherent networks," APL Photonics **9**, 016112 (2024).
160. A. D. Ludlow, X. Huang, M. Notcutt, *et al.*, "Compact, thermal-noise-limited optical cavity for diode laser stabilization at 1×10^{-15}," Opt. Lett. **32**, 641–643 (2007).
161. S. Webster and P. Gill, "Force-insensitive optical cavity," Opt. Lett. **36**, 3572–3574 (2011).
162. D. R. Leibrandt, M. J. Thorpe, M. Notcutt, *et al.*, "Spherical reference cavities for frequency stabilization of lasers in non-laboratory environments," Opt. Express **19**, 3471–3482 (2011).
163. S. Koller, J. Grotti, S. Vogt, *et al.*, "Transportable optical lattice clock with 7×10^{-17} uncertainty," Phys. Rev. Lett. **118**, 073601 (2017).
164. N. Ohmae, M. Takamoto, Y. Takahashi, *et al.*, "Transportable strontium optical lattice clocks operated outside laboratory at the level of 10^{-18} uncertainty," Adv. Quantum Technol. **4**, 2100015 (2021).
165. T. Bothwell, W. Brand, R. Fasano, *et al.*, "Deployment of a transportable Yb optical lattice clock," arXiv (2024).
166. W. Brand, "A transportable ytterbium optical lattice clock with eighteen digits of accuracy," Ph.D. thesis (University of Colorado, 2024).
167. Y. Huang, H. Zhang, B. Zhang, *et al.*, "Geopotential measurement with a robust, transportable Ca^+ optical clock," Phys. Rev. A **102**, 050802 (2020).
168. J. Stuhler, M. Abdel Hafiz, B. Arar, *et al.*, "Opticlock: transportable and easy-to-operate optical single-ion clock," Meas. Sensors **18**, 100264 (2021).
169. J. Cao, J. Yuan, S. Wang, *et al.*, "A compact, transportable optical clock with 1×10^{-17} uncertainty and its absolute frequency measurement," Appl. Phys. Lett. **120**, 054003 (2022).
170. International Clock Oscillator Networking (ICON) Collaboration, "International comparison of optical frequencies with transportable optical lattice clocks," arXiv (2024).
171. S. Dörscher, N. Huntemann, R. Schwarz, *et al.*, "Optical frequency ratio of a $^{171}Yb^+$ single-ion clock and a ^{87}Sr lattice clock," Metrologia **58**, 015005 (2021).
172. T. Lindvall, M. Pizzocaro, R. M. Godun, *et al.*, "Coordinated international comparisons between optical clocks connected via fiber and satellite links," Optica **12**, 843–852 (2025).
173. H. S. Margolis and P. Gill, "Least-squares analysis of clock frequency comparison data to deduce optimized frequency and frequency ratio values," Metrologia **52**, 628–634 (2015).
174. L. Robertsson, "On the evaluation of ultra-high-precision frequency ratio measurements: examining closed loops in a graph theory framework," Metrologia **53**, 1272–1280 (2016).
175. F. Riehle, P. Gill, F. Arias, *et al.*, "The CIPM list of recommended frequency standard values: guidelines and procedures," Metrologia **55**, 188–200 (2018).
176. H. Margolis, G. Panfilo, G. Petit, *et al.*, "The CIPM list 'Recommended values of standard frequencies': 2021 update," Metrologia **61**, 035005 (2024).
177. H. S. Margolis, R. M. Godun, N. Huntemann, *et al.*, "Robust Optical Clocks for International Timescales (ROCIT)," J. Phys. Conf. Ser. **2889**, 012022 (2024).
178. D.-H. Yu, M. Weiss, and T. E. Parker, "Uncertainty of a frequency comparison with distributed dead time and measurement interval offset," Metrologia **44**, 91 (2007).
179. L. Blanchet, C. Salomon, P. Teyssandier, *et al.*, "Relativistic theory for time and frequency transfer to order," Astron. Astrophys. **370**, 320–329 (2001).
180. T. D. Papanikolaou and D. Tsoulis, "Assessment of earth gravity field models in the medium to high frequency spectrum based on GRACE and GOCE dynamic orbit analysis," Geosciences **8**, 441 (2018).
181. H. Denker, L. Timmen, C. Voigt, *et al.*, "Geodetic methods to determine the relativistic redshift at the level of 10^{-18} in the context of international timescales: a review and practical results," J. Geod. **92**, 487–516 (2018).
182. J. Lee, J. H. Kwon, C. Y. Park, *et al.*, "Evaluation of the relativistic redshift in frequency standards at KRISS," Metrologia **61**, 015008 (2024).
183. N. K. Pavlis and M. A. Weiss, "A re-evaluation of the relativistic redshift on frequency standards at NIST, Boulder, Colorado, USA," Metrologia **54**, 535 (2017).
184. C. Voigt, H. Denker, and L. Timmen, "Time-variable gravity potential components for optical clock comparisons and the definition of international time scales," Metrologia **53**, 1365–1383 (2016).
185. C. Grebing, A. Al-Masoudi, S. Dörscher, *et al.*, "Realization of a timescale with an accurate optical lattice clock," Optica **3**, 563–569 (2016).
186. H. Hachisu, F. Nakagawa, Y. Hanado, *et al.*, "Months-long real-time generation of a time scale based on an optical clock," Sci. Rep. **8**, 4243 (2018).
187. J. Yao, J. A. Sherman, T. Fortier, *et al.*, "Optical-clock-based time scale," Phys. Rev. Appl. **12**, 044069 (2019).
188. V. Formichella, L. Galleani, G. Signorile, *et al.*, "Robustness tests for an optical time scale," Metrologia **59**, 015002 (2022).
189. L. Zhu, Y. Lin, Y. Wang, *et al.*, "Preliminary study of generating a local time scale with NIM ^{87}Sr optical lattice clock," Metrologia **59**, 055007 (2022).
190. M. Abgrall, B. Chupin, P. Uhrich, *et al.*, "Optically steered time scale generation at OP and NPL and remote comparisons," J. Phys. Conf. Ser. **2889**, 012024 (2024).
191. W. R. Milner, J. M. Robinson, C. J. Kennedy, *et al.*, "Demonstration of a timescale based on a stable optical carrier," Phys. Rev. Lett. **123**, 173201 (2019).
192. J. Olson, R. W. Fox, T. M. Fortier, *et al.*, "Ramsey-Bordé matter-wave interferometry for laser frequency stabilization at 10–16 frequency instability and below," Phys. Rev. Lett. **123**, 073202 (2019).
193. M. J. Thorpe, L. Rippe, T. M. Fortier, *et al.*, "Frequency stabilization to 6×10^{-16} via spectral-hole burning," Nat. Photonics **5**, 688–693 (2011).
194. E. Cantin, O. Lopez, C. Chardonnet, *et al.*, "REFIMEVE frequency and time network and applications," J. Phys. Conf. Ser. **2889**, 012031 (2024).
195. C. Clivati, R. Aiello, G. Bianco, *et al.*, "Common-clock very long baseline interferometry using a coherent optical fiber link," Optica **7**, 1031–1037 (2020).
196. B. W. Petley, "New definition of the metre," Nature **303**, 373–376 (1983).
197. D. B. Newell, F. Cabiati, J. Fischer, *et al.*, "The CODATA 2017 values of h, e, k, and N_A for the revision of the SI," Metrologia **55**, L13 (2018).
198. J. Lodewyck, "On a definition of the SI second with a set of optical clock transitions," Metrologia **56**, 055009 (2019).
199. M. Takamoto, I. Ushijima, N. Ohmae, *et al.*, "Test of general relativity by a pair of transportable optical lattice clocks," Nat. Photonics **14**, 411–415 (2020).
200. R. F. C. Vessot, M. W. Levine, E. M. Mattison, *et al.*, "Test of relativistic gravitation with a space-borne hydrogen maser," Phys. Rev. Lett. **45**, 2081–2084 (1980).
201. P. Delva, N. Puchades, E. Schönemann, *et al.*, "Gravitational redshift test using eccentric Galileo satellites," Phys. Rev. Lett. **121**, 231101 (2018).
202. S. Herrmann, F. Finke, M. Lülf, *et al.*, "Test of the gravitational redshift with Galileo satellites in an eccentric orbit," Phys. Rev. Lett. **121**, 231102 (2018).
203. A. Bassi, L. Cacciapuoti, S. Capozziello, *et al.*, "A way forward for fundamental physics in space," NPJ Microgravity **8**, 49 (2022).
204. S. Blatt, A. D. Ludlow, G. K. Campbell, *et al.*, "New limits on coupling of fundamental constants to gravity using optical lattice clocks," Phys. Rev. Lett. **100**, 140801 (2008).
205. N. Huntemann, B. Lipphardt, C. Tamm, *et al.*, "Improved limit on a temporal variation of m_p/m_e from comparisons of Yb^+ and Cs atomic clocks," Phys. Rev. Lett. **113**, 210802 (2014).
206. T. Rosenband, D. Hume, P. Schmidt, *et al.*, "Frequency ratio of al+ and hg+ single-ion optical clocks; metrology at the 17th decimal place," Science **319**, 1808–1812 (2008).

207. B. M. Roberts, P. Delva, A. Al-Masoudi, *et al.*, "Search for transient variations of the fine structure constant and dark matter using fiber-linked optical atomic clocks," New J. Phys. **22**, 093010 (2020).
208. M. Filzinger, S. Dörscher, R. Lange, *et al.*, "Improved limits on the coupling of ultralight bosonic dark matter to photons from optical atomic clock comparisons," Phys. Rev. Lett. **130**, 253001 (2023).
209. N. Sherrill, A. O. Parsons, C. F. A. Baynham, *et al.*, "Analysis of atomic-clock data to constrain variations of fundamental constants," New J. Phys. **25**, 093012 (2023).
210. S. Kolkowitz, I. Pikovski, N. Langellier, *et al.*, "Gravitational wave detection with optical lattice atomic clocks," Phys. Rev. D **94**, 124043 (2016).
211. M. Kozlov, M. Safronova, J. Crespo López-Urrutia, *et al.*, "Highly charged ions: optical clocks and applications in fundamental physics," Rev. Mod. Phys. **90**, 045005 (2018).
212. V. V. Flambaum, "Enhanced effect of temporal variation of the fine structure constant and the strong interaction in ^{229}Th," Phys. Rev. Lett. **97**, 092502 (2006).
213. T. E. Mehlstäubler, G. Grosche, C. Lisdat, *et al.*, "Atomic clocks for geodesy," Rep. Prog. Phys. **81**, 064401 (2018).
214. P. Gillot, O. Francis, A. Landragin, *et al.*, "Stability comparison of two absolute gravimeters: optical versus atomic interferometers," Metrologia **51**, L15 (2014).
215. G. Lion, I. Panet, P. Wolf, *et al.*, "Determination of a high spatial resolution geopotential model using atomic clock comparisons," J. Geod. **91**, 597–611 (2017).
216. J. Grotti, S. Keller, S. Vogt, *et al.*, "Geodesy and metrology with a transportable optical clock," Nat. Phys. **14**, 437–441 (2018).
217. T. Bothwell, C. J. Kennedy, A. Aeppli, *et al.*, "Resolving the gravitational redshift across a millimetre-scale atomic sample," Nature **602**, 420–424 (2022).
218. B. L. S. Marlow and D. R. Scherer, "A review of commercial and emerging atomic frequency standards," IEEE Trans. Ultrason. Ferroelectr. Freq. Control **68**, 2007–2022 (2021).
219. B. R. White, R. F. Offer, A. P. Hilton, *et al.*, "The SWAP plot: visualising the performance of portable atomic clocks as a function of their size, weight and power," arXiv (2024).
220. J. D. Roslund, A. Cingöz, W. D. Lunden, *et al.*, "Optical clocks at sea," Nature **628**, 736–740 (2024).
221. A. P. Hilton, R. F. Offer, E. Klantsataya, *et al.*, "Demonstration of a mobile optical clock ensemble at sea," Nat. Commun. **16**, 6063 (2025).
222. K. Döringshoff, F. B. Gutsch, V. Schkolnik, *et al.*, "Iodine frequency reference on a sounding rocket," Phys. Rev. Appl. **11**, 054068 (2019).
223. J. Kitching, M. Hummon, W. McGehee, *et al.*, "Next-generation chip scale atomic clocks," J. Phys. Conf. Ser. **2889**, 012015 (2024).
224. L. Chang, S. Liu, and J. E. Bowers, "Integrated optical frequency comb technologies," Nat. Photonics **16**, 95–108 (2022).
225. T. D. Shoji, W. Xie, K. L. Silverman, *et al.*, "Ultra-low-noise monolithic mode-locked solid-state laser," Optica **3**, 995–998 (2016).
226. Y. Liu, D. Lee, T. Nakamura, *et al.*, "Low-noise microwave generation with an air-gap optical reference cavity," APL Photonics **9**, 010806 (2024).
227. W. Loh, J. Stuart, D. Reens, *et al.*, "Operation of an optical atomic clock with a Brillouin laser subsystem," Nature **588**, 244–249 (2020).
228. W. Loh, D. Reens, D. Kharas, *et al.*, "Optical atomic clock interrogation using an integrated spiral cavity laser," Nat. Photonics **19**, 277–283 (2025).
229. K. Dietze, L. Pelzer, L. Krinner, *et al.*, "Entanglement-enhanced optical ion clock," arXiv (2025).
230. B. C. Nichol, R. Srinivas, D. Nadlinger, *et al.*, "An elementary quantum network of entangled optical atomic clocks," Nature **609**, 689–694 (2022).
231. J. M. Robinson, M. Miklos, Y. M. Tso, *et al.*, "Direct comparison of two spin-squeezed optical clock ensembles at the 10^{-17} level," Nat. Phys. **20**, 208–213 (2024).
232. G. Zhao, J. Xia, Y. Liu, *et al.*, "Laser cooling alkaline-earth atoms for optical clock in Chinese space station," Chin. Phys. Lett. **42**, 063701 (2025).
233. A. Derevianko, K. Gibble, L. Hollberg, *et al.*, "Fundamental physics with a state-of-the-art optical clock in space," Quantum Sci. Technol. **7**, 044002 (2022).